frontiers | Frontiers in Marine Science

ORIGINAL RESEARCH
published: 11 May 2022
doi: 10.3389/fmars.2022.863245

Revisit the Sedimentary Stratigraphic Evolution and Environmental Changes on the Outer Shelf of the East China Sea Since MIS 5

Zhongbo Wang[1,2], Shouye Yang[3], Haiyan Tang[1], Yilin Zheng[1], Hongyue Wang[1], Zhixun Zhang[4], Yong Zhang[2,4], Xi Mei[2,4], Qiang Wang[5] and Zhongping Lai[1,6]*

[1] Institute of Marine Sciences, Guangdong Provincial Key Laboratory of Marine Disaster Prediction and Prevention, Shantou University, Shantou, China, [2] Laboratory for Marine Mineral Resources, Pilot National Laboratory for Marine Science and Technology, Qingdao, China, [3] State Key Laboratory of Marine Geology, Tongji University, Shanghai, China, [4] Key Laboratory of Marine Hydrocarbon Resources and Environmental Geology, Ministry of Natural Resources, Qingdao Institute of Marine Geology, Qingdao, China, [5] Tianjin Institute of Geology and Mineral Resources, Tianjin, China, [6] Southern Marine Science and Engineering Guangdong Laboratory (Zhuhai), Zhuhai, China

OPEN ACCESS

Edited by:
Zhan Hu,
Sun Yat-sen University, Zhuhai Campus, China

Reviewed by:
Yuan-Pin Chang,
National Sun Yat-sen University, Taiwan
Jeroen Groeneveld,
University of Hamburg, Germany

***Correspondence:**
Zhongbo Wang
zhbwang@stu.edu.cn

Specialty section:
This article was submitted to Coastal Ocean Processes, a section of the journal Frontiers in Marine Science

Received: *27 January 2022*
Accepted: *11 April 2022*
Published: *11 May 2022*

Citation:
Wang Z, Yang S, Tang H, Zheng Y, Wang H, Zhang Z, Zhang Y, Mei X, Wang Q and Lai Z (2022) Revisit the Sedimentary Stratigraphic Evolution and Environmental Changes on the Outer Shelf of the East China Sea Since MIS 5. Front. Mar. Sci. 9:863245. doi: 10.3389/fmars.2022.863245

The East China Sea (ECS) is featured by the broad continental shelf, huge terrigenous sediment input and striking river-sea interaction during the Quaternary. Despite the numerous studies, mostly on the delta, coastal and inner shelf areas, the late Quaternary stratigraphy and sedimentary environment on the mid-outer ECS shelf were poorly documented. In particular, it is still controversial in issues such as the recognition of marine transgression deposits in the interglacial period and the occurrence and ages of deposits in the glacial period. This study presents new data of high-resolution seismic reflection profiles and collective evidences from lithology, microfossil assemblages and geochronology of borehole SFK-1 on the ECS outer shelf, aiming to revisit the sedimentary stratigraphic evolution and environmental changes since the Marine Isotopic Stage 5 (MIS 5). Sixty-one ages were obtained by radiocarbon and Optical Stimulation Luminescence (OSL), providing robust constraints on the chronostratigraphy. Three marine regression/transgression cycles were identified, which primarily constrained the sedimentary environmental evolution over the past 100 kyrs. Although the strong river-sea interaction accompanied with sea level fluctuations characterized the late Quaternary depositional environment on the shelf, this study clearly identified the stratigraphic boundaries between MIS 1 and MIS 5, and confirmed the tide-influenced fluvial deposition formed during the Last Glacial Maximum on the outer shelf. We infer that tidal forcing significantly superimposed its influence on sea level change and thus formed the most striking feature on the late Quaternary stratigraphy of the open ECS shelf. With the combination of a large number of absolute depositional ages with high-resolution core records, the major findings of this study may allow better understanding of the Quaternary sedimentary evolution and river-sea interaction on open shelves dominated by siliciclastic sedimentation.

Keywords: East China Sea, drilling core, chronology, late Quaternary stratigraphy, paleoenvironment, land-sea interaction

1 INTRODUCTION

The East China Sea (ECS), a typical marginal sea of the west Pacific Ocean, is featured by one of the widest and gentlest shelves in the world, with huge sedimentation accommodation space (Li et al., 2014a; Yang et al., 2016). A large volume of siliciclastic sediments have accumulated on the broad shelf and continental slope, which originate from the two large rivers, Changjiang (Yangtze River) and Huanghe (Yellow River), and small mountainous rivers such as those in Taiwan Island. During the last glacial and interglacial periods, the flux and deposition of detrital and fluvial sediments in the sea were predominantly controlled by monsoon climate, sea-level fluctuation, and ocean circulation (Li et al., 2014a; Yang et al., 2014; Yang et al., 2016). During the Last Glacial Maximum (LGM) the coastline of ECS retreated to its furthest position towards the shelf break, with the sea level dropping about 120 m below the present one (Emery et al., 1971; Qin et al., 1987; Saito, 1998a; Liu and Milliman, 2004a; Li et al., 2005a and Li et al., 2014a; Liu et al., 2021). After the LGM, the sea level began to rise and reached the highstand at present position at ca. 7 ka. Correspondingly, large scale sandy and muddy sedimentary systems respectively formed on the mid-outer and inner shelves during the last transgression with the sea level rise, which are defined as transgressive systems tract (TST) and highstand systems tract (HST), respectively (Liu et al., 2007a; Li et al., 2009; Li et al., 2014a). Therefore, the sequence stratigraphy on the ECS shelf witnessed the changes in paleoenvironment and sea level during the late Quaternary. The ECS shelf could thus be regarded as a natural laboratory for the studies of sea level fluctuation, river-sea interaction, and sedimentary system development on the open shelf with abundant terrigenous sediment supply.

During the past two decades, most previous studies on the late Quaternary stratigraphy framework and paleoenvironmental changes of the ECS were confined on the inner shelf and in the Changjiang estuarine and delta areas, while the mid-outer shelf was rarely concerned mostly because of the sever investigation condition and technical limitation (Chen et al., 2000; Hori et al., 2002; Li et al., 2002b; Wang et al., 2005; Liu et al., 2007b; Zhao et al., 2008; Gao and Collins, 2014; Li et al., 2014a; Bi et al., 2017; Cong et al., 2021). The pioneer investigation on the middle ECS shelf carried out by Yang (1989) constructed a model of sedimentary stratigraphy evolution during the late Pleistocene based on the microfossil and pollen assemblages in borehole YQ1 (**Figure 1**), but the chronostratigraphy of this borehole was poorly constrained without absolute depositional ages. To date, the sequence stratigraphy during the last deglacial and Holocene period was primarily reconstructed on the mid-outer ECS shelf based on the high-resolution core records and shallow seismic profiles (Saito et al., 1998b; Yoo et al., 2002; Uehara and Saito, 2003; Wang et al., 2013; Wang et al., 2014; Xu et al., 2018; Xu et al., 2020).

In 1990s, the most representative research progresses on the stratigraphy of the outer ECS shelf were made by the joint cruise of China and France in 1996, and marine geological investigation by Shanghai Geological Survey in 1990. The high-resolution single-channel seismic survey was conducted in combination

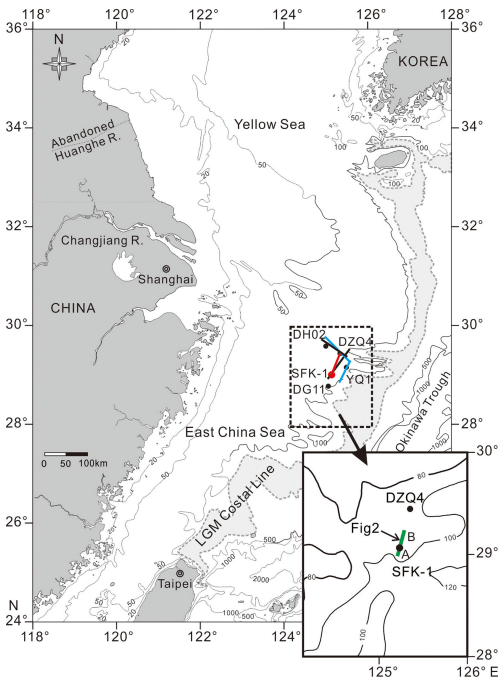

FIGURE 1 | A sketch map of the East China Sea (ECS) with the locations of core SKF-1 and other boreholes, and seismic mentioned in this study. The index map shows the seismic track line A-B across the studied core (see **Figure 2** for the details). The black, blue and red solid lines are seismic track lines in Liu et al. (2000)/Berné et al. (2002), Xu et al. (2020), and this study, respectively. The green solid line is the selected part of the profile cross SFK-1 and DZQ4. The coastal line (gray shaded area) at the last glacial maximum (LGM) is modified after Saito et al. (1998a).

with acquiring of core records such as on borehole DZQ4. Mostly based on these previous investigations, the stratigraphic sequences of transgression–regression were established (Tang, 1996; Saito et al., 1998b; Liu et al., 2000; Berné et al., 2002; Yoo et al., 2002; Wu et al., 2010), and the formation mechanisms of tidal sand ridges on the open shelf were discussed (Li et al., 2002a; Yang, 2002; Wellner and Bartek, 2003; Wu et al., 2005; Liu et al., 2007a). Recently, Xu et al. (2020) studied the sedimentary stratigraphy of borehole DH02 (100 m) and seismic profiles on the outer shelf of ECS, and identified three sequences corresponding to glacial-interglacial sea-level cycles of Marine Isotopic Stages (MIS) 1-2, 3-6, and 7-8, and further established seven sedimentary facies since MIS 8. Meanwhile, Jiang et al. (2020) established an age model and chronological framework for the late Quaternary strata, based on paleomagnetic parameters of the core SFK-1 from ECS outer shelf. In addition, authigenic iron sulfides were used to indicate the sedimentary environments and sea-level change since MIS 3 on the ECS (Liu et al., 2021). Overall, the lack of high-precision absolute dating on the sedimentary strata greatly hampered the precise correlation between different stratigraphic records on the mid-outer shelf.

In the following sections, we will review the state-of-the-art research progress and key questions remained on the late

Quaternary sedimentary stratigraphy on the ECS, and present new data from the *in-situ* geophysical observations and comprehensive analysis of a borehole with the high-resolution dating constraint.

2 KEY QUESTIONS RELATED TO THE LATE QUATERNARY SEDIMENTARY STRATIGRAPHY ON THE OPEN SHELF OF ECS

Although previous studies have well documented the depositional sequences and sedimentary facies in response to sea level changes during the late Quaternary, some fundamental and key questions, which are related to the stratigraphy and paleoenvironmental changes of the mid-outer ECS shelf, remain controversial. For instance, two contrasting opinions exist on the late Quaternary stratigraphic framework on the outer shelf, based on the seismic survey and geochronology especially the thermoluminescence (TL) ages (**Figure 1**). Some studies suggest that the glacial strata of MIS 2 and MIS 4 were hardly preserved on the dynamic shelf environment mainly because of the limited accommodation space within the glacial periods and the winnowing erosion during subsequent marine transgressions. Even the MIS 2 deposits, preserved on the shelf, are too thin to be clearly recognized from the seismic profiles. In contrast, the strata formed in interglacial intervals, such as MIS 5, were well recognized on the outer shelf of ECS because of the ample accommodation space for sediment accumulation, and the abundant supply of terrigenous sediments from surrounding landmass under favorable monsoon climates. However, it was challenging to fingerprint the detailed stratum of MIS 5 because of the subsequent erosion in MIS 4. Despite the strong sea-level fall during MIS 6 causing strong fluvial headward erosion on the exposed surface, the well-developed deposits of MIS 5 could survive and be well recognized from the seismic stratigraphy and thus, be regarded as a key and diagnostic sequence in the late Pleistocene stratigraphy studies on the ECS shelf (Liu et al., 1999; Liu et al., 2000; Liu et al., 2003; Wu et al., 2010; Xu et al., 2020).

By combining more lines of evidences from different cores as well as seismic data, the other studies, however, argue that the late Quaternary sedimentary strata on the outer shelf were almost continuous and mainly composed of depositions of MIS 1, MIS 2, MIS 3-5.2, MIS 5.3-5.5, and MIS 6, which suggest that the deposition of glacial period was well preserved and recognized on the open shelf (Berné et al., 2002; Li et al., 2002a; Yu et al., 2006; Wang et al., 2013; Wang et al., 2014; Xu et al., 2020). In addition, the MIS 5 strata was well developed and more easily recognized than the MIS 3 strata probably because of different extents of marine transgression and terrigenous sediment accumulation (Berné et al., 2002; Xu et al., 2020). The paleo-deltaic and estuarine sediments accumulated during the LGM were preserved on the outer shelf, despite the bypassing effect during the sediment routing process in the lowstand of sea level (Li et al., 2002a; Yu et al., 2006; Wang et al., 2013; Wang et al., 2014; Xu et al., 2018).

Recent studies summarized the stratigraphic evolution on the outer shelf of the ECS during the last glacial period (Yang, 2002; Li et al., 2005b, Wang et al., 2013; Li et al., 2014a; Wang et al., 2014; Xu et al., 2018; Xu et al., 2020). Three distinct transgressive strata (MIS 1, 3 and 5) can be recognized, and the strata of MIS 3 and 5 were well preserved on the shelf and can be well correlated between the Bohai Sea, Yellow Sea and East China Sea (Yang et al., 1996). The deglacial sea-level rise is characterized by forming much variable sedimentary systems on these shelves, including tidal sand ridges on the mid-outer ECS shelf, muddy depositional systems on the inner ECS shelf and other shelves (Saito et al., 1998b; Yoo et al., 2002; Uehara and Saito, 2003; Wang et al., 2013; Wang et al., 2014; Xu et al., 2018). The different stages of sea level rise, local hydrodynamic conditions and terrigenous sediment inputs co-governed the Holocene sedimentation on these shelves (Li et al., 2014a).

In summary, numerous previous studies focused on the Changjiang delta and inner shelf areas of the ECS, among which the stratigraphy, sedimentation process and paleoenvironmental changes during the Holocene were well documented. While, the stratigraphic structure and sedimentary environments on the mid-outer ECS shelf during the late Quaternary remain poorly known, mainly because of the absence of reliable chronology leading to the lack of combining various lines of evidences. In the previous studies, the recognition and differentiation of the late Quaternary strata were predominantly based on the paleogeographic interpretation and seismic reflection profiles, which caused unpredictable uncertainties. To target these challenges, we aim to reconstruct the late Quaternary stratigraphy and depositional environmental evolution on the outer ECS shelf since MIS 5, based on the comprehensive studies of sedimentary facies, biostratigraphy and chronostratigraphy of the borehole SFK-1, and on the comparison with the high-resolution seismic profile data. Previously, we have reported the paleo-fluvial sedimentation in this borehole during the LGM (Wang et al., 2013; Wang et al., 2014), and this study will establish the late Quaternary stratigraphic framework with more robust chronological constraints. To our knowledge, this work will be pioneering in terms of the high-resolution chronostratigraphy on the outer ECS shelf, and thus will be contributive to better understanding the late Quaternary river-sea interaction and paleoenvironmental variability in this unique marginal sea.

3 MATERIALS AND METHODS

For this study, a borehole named SFK-1 was taken from the outer shelf of ECS (29°03.15′N, 125°15.30′E) at 88.3 m water depth in October, 2007, by D/V Kan 407 from the First Marine Geological Investigation Team of Shanghai Geological Survey (**Figure 1**, Wang et al., 2014). The core is 82.9 m long and the average recovery rate is 89%.

3.1 Lithological Description and Grain Size Analysis

The sediment core was split, described, photographed and subsampled in the laboratory. Lithological description includes color, texture, lithology, macrofossil assemblage, bioturbation,

and sedimentary structure. The subsamples were collected with intervals at 20 cm for grain size measurement, and at 10–15 cm for microfossil examination. For grain size analysis, the subsamples were pretreated with 10% H_2O_2 and 0.1 N HCl to remove organic matter and carbonate, respectively. A total of 398 samples were measured with the Mastersizer-2000 laser particle size analyzer in the laboratory of Qingdao Institute of Marine Geology. The grain size parameters were presented with the method of Folk and Ward (1957).

For microfossil analyses, 198 samples were conducted by the standard method (Wang et al., 1985). The samples were oven-dried at 60°C, weighed and soaked in distilled water for 24 hours to disaggregate before sieving with a 63 μm mesh, and only the fraction ≥63 μm of each 50 g dry sample was examined under the optical microscope. Foraminifera including benthic and planktonic species were recognized, following the method by Wang et al. (1985; 1988). Foraminifera assemblages have been analyzed on the basis of species abundance, and the proxies of simple diversity (number of species) and Shannon-Weiner index (complex diversity, distribution uniformity of foraminifera, Shannon and Wiener, 1949) were also used for the indication of depositional environment (Wang et al., 1988).

3.2 Establishing the Chronostratigraphy

For construction of reliable chronostratigraphy, we adopted various dating methods, including radiocarbon dating of 17 samples and Optical Stimulation Luminescence (OSL) dating of 44 samples. All the dates are given in **Table 1** (^{14}C) and **Table 2** (OSL).

Three molluscan shell samples were dated using Accelerator Mass Spectrometry (AMS) in the AMS Laboratory at Peking University, and three microfossil samples (a benthic foraminifera: *Ammonia beccarii* vars.) in Woods Hole Oceanographic Institution, USA. The other 11 samples of molluscan fragments or peat were measured by low background liquid flash spectrometer (1220 type, Finland). All dates were calibrated to calendar ages using the procedure Calib Rev 8.1.0 with the latest calibration database IntCal20 (Reimer et al., 2020) and Marine20 (Heaton et al., 2020). The calibrated ages were reported as calendar ^{14}C ages before 1950 AD (cal. a BP) with 95.4% calibrated range (**Table 1**). Radiocarbon ages were calibrated to remove region marine reservoir effects (ΔR= −165 ± 30yr), as determined for the East China Sea by Yoneda et al. (2007).

A total of 44 samples were dated by OSL (**Table 2**). The samples for OSL dating, being 20 cm long core sediment, were preferentially and quickly collected from the core and completely packed by aluminum foil. After being put in the hermetic plastic bags, they were preserved in the seal box. Only those relatively continuous and unbroken whole sediment segments were considered for the OSL dating, for making sure the *in situ* deposition and no obvious disturbance. In the lab, all the sample preparation was conducted under the subdued red light. The outer 2-4 cm of each end was removed. The central portion was used for further processes, including the pretreatment with 10% HCl (to remove carbonates), 38% H_2O_2 (to remove organic matter), and separation for the 4-11 μm size fraction by settling following the Stoke's Law. The 4-11 μm fractions were etched with 35% hydrofluorosilicic acid (H_2SiF_6) for 1 week to dissolve feldspars and subsequently treated with 10% HCl to remove acid-soluble fluoride precipitates (Lai, 2010; Xu et al., 2020). The purified quartz grains were then mounted on stainless steel discs using ethanol prior to measurement. The purity of the extracted quartz grains was checked using IRSL stimulation (Duller, 2003).

TABLE 1 | The radiocarbon (^{14}C) ages obtained by traditional and AMS methods on selected samples from borehole SFK-1 (calibrated ages).

Lab codes	Depth (mbsf)	Dating materials	Age (a B.P.)	Calibrated age(95.4% calibrated range; cal. a BP)	Calendar age (cal. a B.P.)
2008y898	0.57	Molluscan shell	5 300 ± 170	4122-3312	3717
BA10815	0.70	Molluscan shell (*Clausinella isabellina*, Philippi, 1849)	4 140 ± 25*	2468-2106	2287
2008y899	1.11	Molluscan shell	3 000 ± 150	1256-441	849
OS-85045	1.20	Benthic foraminifera	2 740 ± 40*	742-377	560
BA10814	2.80	Molluscan shell(*Solenidae*)	7255 ± 45*	5735-5456	5596
2008y900	2.99	Molluscan shell	5 600 ± 350	4825-3247	4036
OS-85032	3.80	Benthic foraminifera	3 770 ± 30*	1976-1608	1792
BA10813	4.56	Molluscan shell	9420 ± 40*	8546-8184	8365
2008y901	5.26	Molluscan shell	5 500 ± 100	4190-3644	3917
2008y905	14.93	Molluscan shell	17 000 ± 600	19363-16514	17939
2008y906	15.63	Molluscan shell	>20 000		
2008y907	16.73	Molluscan shell	18 500 ± 800	21454-17768	19611
2008y908	24.83	Molluscan shell	22 000 ± 900	25339-21690	23515
OS-85030	28.80	Benthic foraminifera	41 000 ± 400*	42129-40810	41470
2008y909	29.09	Dark mud	28 000 ± 1300	32331-27117	29724
2008y912	30.03	Molluscan shell	27 000 ± 900	30514-26713	28612
2008y915	31.90	Dark mud	>31 000		

**AMS^{14}C sample; 'OS' samples were measured by AMS laboratory in the Woods Hole Oceanographic Institution (WHOI). 'BA' samples were measured by the AMS laboratory at Peking University. The others were measured by the Laboratory of Qingdao Institute of Marine Geology, China, using the traditional method.*

TABLE 2 | The OSL dates of selected samples from borehole SFK-1.

Samples	Depth (mbsf)	U(10^{-6})	Th(10^{-6})	K_2O (%)	Moisture content (%)	*AD* (Gy)	*d* (Gy/ka)	*T* (ka)
OSL1	5.8	3.44	23.0	2.08	27	35.4	5.06	7 ± 0.7
OSL2	6.6	1.93	9.1	1.93	24	34.6	3.84	9 ± 0.9
OSL3	7.4	1.89	10.5	2.26	27	39.8	3.98	10 ± 1
OSL4	8.4	2.10	12.9	2.12	27	41.1	3.74	11 ± 1
OSL5	9.8	2.18	13.1	2.49	48	44.2	3.84	11.5 ± 1
OSL6	10.9	2.48	13.6	2.61	37	45.2	3.62	12.5 ± 1
OSL7	11.9	1.97	12.2	2.27	37	45	3.46	13 ± 1
OSL8	14.1	2.17	13.7	2.25	23	48.5	3.23	15 ± 2
OSL9	16	3.23	13.6	2.08	23	53.4	2.97	18 ± 2
OSL10	17.5	1.39	9.1	2.05	22	62.9	3.31	19 ± 2
OSL11	18.4	1.70	10.7	2.13	34	69.6	3.48	20 ± 2
OSL12	19.3	1.55	9.0	2.01	28	74.6	3.24	23 ± 2
OSL13	20.3	1.74	10.0	1.89	23	82.3	3.29	25 ± 3
OSL14	22.8	1.57	8.3	2.20	25	98.7	3.53	28 ± 3
OSL15	23.7	1.09	9.4	1.98	20	95.2	3.17	30 ± 3
OSL16	25.6	1.76	10.6	2.06	24	102.7	3.21	32 ± 3
OSL17	27.4	1.59	10.7	2.04	23	121.2	3.56	34 ± 3
OSL18	29.1	2.54	14.9	2.83	36	158.7	4.53	35 ± 4
OSL19	30.4	2.41	14.5	2.78	35	189.7	4.63	41 ± 4
OSL20	33	2.63	15.7	3.00	43	205.9	4.68	44 ± 4
OSL21	34.3	2.75	13.5	2.58	35	211.1	4.49	47 ± 5
OSL22	35.1	2.72	14.3	2.47	31	238.8	4.87	49 ± 5
OSL23	36.3	3.47	18.2	1.93	24	261.6	5.45	48 ± 5
OSL24	38.5	2.61	15.0	2.41	29	256.9	5.14	50 ± 5
OSL25	39.3	2.05	10.9	2.04	27	210.6	3.97	53 ± 5
OSL26	40.4	2.23	11.7	1.96	27	262.4	4.69	56 ± 6
OSL27	42.1	4.06	10.4	1.92	27	289.4	5.08	57 ± 6
OSL28	44.1	1.86	11.7	2.02	24	227.5	4.06	56 ± 6
OSL29	47.3	1.89	10.5	1.83	22	231.9	4.00	58 ± 6
OSL30	48.9	2.51	14.2	2.14	23	289.4	4.82	60 ± 6
OSL31	53.2	3.25	17.1	2.77	26	353.6	5.80	61 ± 6
OSL32	55.1	2.62	16.3	2.90	30	328.3	5.47	60 ± 6
OSL33	55.9	2.92	16.1	2.83	27	348.3	5.62	62 ± 6
OSL34	61	4.42	20.6	2.89	30	412.6	6.35	65 ± 6
OSL35	67.8	3.08	15.7	2.53	24	361.8	5.57	75 ± 8
OSL36	73.5	2.90	13.5	2.57	25	387.1	5.87	66 ± 7
OSL37	74.2	2.48	13.0	2.53	25	362.8	5.26	69 ± 7
OSL38	75.8	3.43	17.4	2.80	33	356.1	5.74	62 ± 6
OSL39	76.6	3.37	16.3	2.86	30	392.8	5.78	68 ± 7
OSL40	78.6	3.17	17.0	2.94	31	358.8	5.70	63 ± 6
OSL41	79.4	3.15	16.2	2.72	32	375.5	5.07	74 ± 7
OSL42	79.8	2.97	16.3	2.95	31	371.3	4.76	78 ± 8
OSL43	80.5	2.72	13.5	2.70	39	375.6	4.70	80 ± 8
OSL44	81.7	3.56	16.9	3.11	33	485.5	5.34	91 ± 9

AD, accumulated dose; d, dose; T, dates.

All the OSL measurements were preformed using an automated Daybreak 2200 OSL reader equipped with infrared (880 ± 60 nm) and blue (470 ± 5 nm) LED units and a $^{90}Sr/Y$ beta source for irradiation. The quartz grains were stimulated at 125 °C with blue LEDs for 1 min, and the OSL signal was detected using an EMI 9235QA photomultiplier tube coupled in front with two 3-mm U-340 (290-370 nm) glass filters.

In this study, the single-aliquot regenerative-dose (SAR) OSL dating method (Murray and Wintle, 2003) was applied to fine-grained (4-11μm) quartz samples. And the net OSL signal was calculated using the first 2-s integral of the OSL decay curve minus the last 2 s integral for equivalent dose (D_e) determination.

For doserate measurement, samples were sent for chemical elements (U, Th, and K) detection after the water content measurement. The concentrations of U and Th were measured by the inductively coupled plasma mass spectrometry (ICP-MS), and the concentrations of K by inductively coupled plasma-optical emission spectrometry (ICP-OES). The concentrations of U, Th and K in these samples are displayed in **Table 2**. Calculation of the cosmic dose rate was based on Prescott and Hutton (1994).

Both the traditional ^{14}C and OSL dating were conducted in the laboratory of Qingdao Institute of Marine Geology, China Geological Survey (CGS).

3.3 Seismic Survey and Sub-Bottom Profile Acquirement

In this paper, the section (A–B) of the profile across boreholes DZQ4 and SFK-1 was selected for the interpretation of

sedimentary structure (**Figure 1**), which is located very close to the seismic profile distribution of previous studies (Liu et al., 2000; Berné et al., 2002; Liu et al., 2003; Wellner and Bartek, 2003; Xu et al., 2018). In the field survey, a SIG 2 Mille sub–bottom profiler was employed, with a Boomer system for shooting and Delph seismic system for data acquisition. The depth conversion was calculated using an average sound velocity of 1650 m/s, as reported in previous studies (Yang, 1989; Liu et al., 2000; Berné et al., 2002). High-resolution seismic interpretation was based on the recognition of minor seismic discontinuities by comparing the seismic facies with the lithofacies of core SFK-1.

4 RESULTS

4.1 Seismic Reflections and Units Across Cores SFK-1 and DZQ4

A total of 10 seismic units were identified in the high-resolution seismic profile A-B (**Figure 2**) across cores SFK-1 and DZQ4 based on the seismic reflection features and their contacts. The main characteristics of these seismic units are summarized in **Figure 2** and also sees below. Numbers have been attributed to every major seismic unit (SU1 to SU10, from top to bottom), the underlying discontinuity being labeled with a 'D' followed by the corresponding number.

SU10: Due to the interference of multiple reflections, it is difficult to identify its bottom reflection layer, and the top layer is D9. The unit has relatively steep clinoform that systematically dips toward the SW, being toplap with the overlying layer of SU9 and locally distributed in the study area.

SU9: It displays horizontal and continuous distribution, with low frequency and strong amplitude. SU9 as a seismic subunit displays continuous internal reflections, with a high frequency and relatively weak amplitude, forming a low-angle onlap fill at the bottom. SU9 has a conformable contact with the overlying layer of SU8, and is widely distributed in the study area.

SU8: It displays continuously with a high frequency and weak amplitude, subparallel distribution on the outer shelf. It has been eroded by the overlying layer of SU7 and forming a parallel unconformity contact with the SU9.

SU7: This seismic unit displays a wide distribution, with subparallel and continuous high frequency and weak amplitude, being a toplap and truncated with the overlying layer of SU6.

SU6: This unit shows a parallel, onlap and continuous distribution, and has a low frequency and high amplitude, an angular unconformity contact with the SU7.

SU5: A large variation in distribution patterns characterizes this unit, with chaotic reflections and clinoform reflections.

SU4: This unit is characterized by a high amplitude and continuous and wide distribution, with partly channelized erosion. SU4 has an erosion contact with the overlying SU3.

SU3: This unit is filled by the chaotic reflections, with erosional contacts between the overlying SU2 and underlying SU4. The upper interface is continuous, subparallel and widely distributed. Typical fluvial seismic reflections can be observed in this unit (SU3-1~SU3-3), displaying apparently lateral aggradation.

SU2: A clear planation surface occurs between SU2 and SU1, which is truncated and partly onlap. SU2-2 is horizontal and sub-horizontal, and SU2-1 developed striking foreset inclined bedding.

SU1: This unit is affected heavily by the multiple seabed reflection. It is hard to identify D1 from the overlying layer.

4.2 Lithological Description and Sedimentary Units of Core SFK-1

Based on the sediment color, texture, structure, grain size composition and microfossil assemblages, eleven sedimentary units (LU10 to LU1) are recognized from bottom to top (**Figures 3**–**5**). The lithological description of each depositional unit is summarized below.

LU10 (82.9–82.4 mbsf, meter below seafloor): The bottom unit was poorly recovered during the drilling, showing grey silt mixed with grey medium-fine sand at the core cut. No erosional surface and distinct sedimentary structure can be observed.

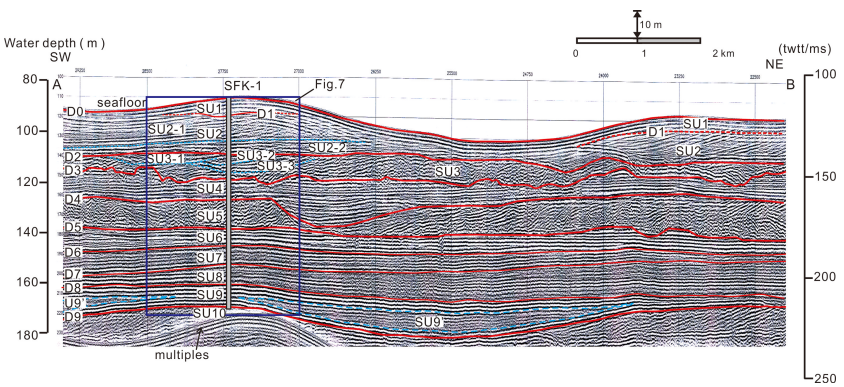

FIGURE 2 | The **(A, B)** section of the high-resolution seismic profile across boreholes SFK-1 and DZQ4. The schematic interpretation is partly modified after Wang et al. (2013; 2014). The red solid and blue dotted lines are the boundaries of depositional units and subunits respectively. SU indicates seismic units, and D denotes the discontinuity or depositional hiatus.

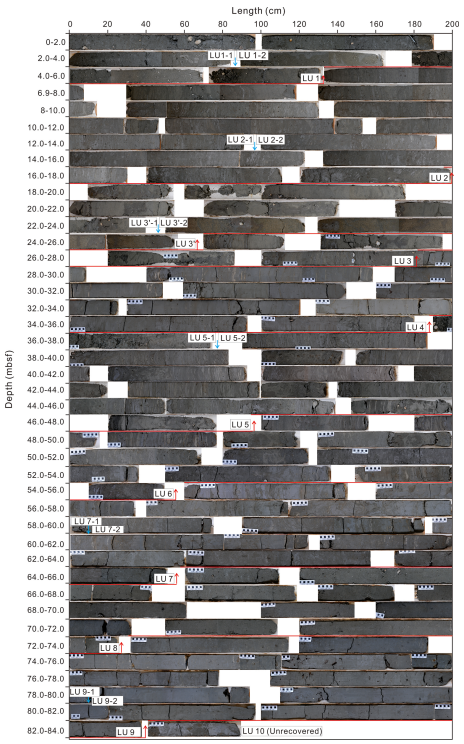

FIGURE 3 | The photos showing the sediment characters and lithological units of borehole SFK-1. mbsf, meters below sea floor. The red and blue arrows indicate the boundaries of depositional units and subunits respectively.

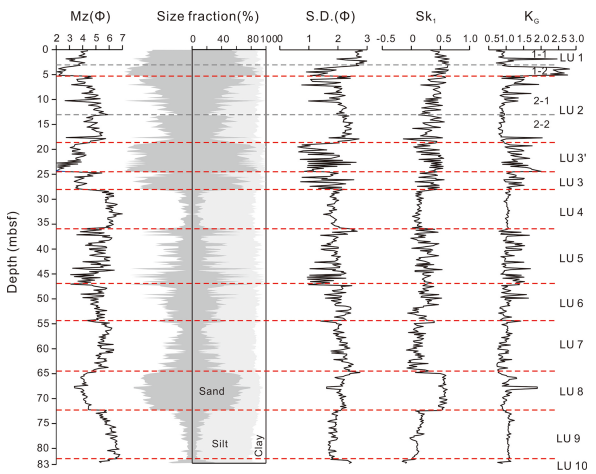

FIGURE 4 | The grain size composition of borehole SFK-1. Mz, mean grain size (phi); S.D., standard deviation; Sk_I, skewness; K_G, kurtosis.

LU9 (82.4–72.3 mbsf): The sediments are dominated by grey silt with a trend of coarsening upward, massive bedding and heavily bioturbation occur in the top part. This unit is divided into two subunits, LU9-1 (78.1–72.3 mbsf) and LU9-2 (82.4–78.1 mbsf), based on the internal sedimentary characters and microfossil assemblages. Some burrows are found in the sediments of LU9-1, and molluscan fragments occur in LU9-2. The mean grain size (Mz) varies from 6 Φ to 4 Φ, with the content of sand less than 20%. The assemblages of microfossils change considerably between two subunits with almost the same benthic-planktonic ratio. The dominant species of LU9-1 include *Protelphidium tuberculatum*, *Ammonia beccarii* vars. and *Episominella naraensis*, while *Bolivina robusta-Globocassidulina subglobosa-Protelphidium tuberculatum* characterize the microfossil assemblages in LU9-2. Their common species are *Brizalina striatula*, *Nonionella decora*, *Nonion akitaense* in LU9-1 and *Epistominella naraensis*, *Elphidium advenum*, *Cassidulinia carinata* in LU9-2, respectively.

LU 8 (72.3–64.7 mbsf): The sediments consist of grey to black medium-fine sand, showing massive bedding and bioturbation upward. The molluscan fragments increase toward the top, meanwhile, the sediment color changes from dark and grey to celadon. The Mz ranges from 3 Φ to 4 Φ, and sand contents exceed 50% in all samples, with a stable and striking positive skewness. The foraminifera assemblages vary considerably, with the main species being *Protelphidium tuberculatum*, *Bolivina robusta*, *Nonionella decora*, while *Pulleniatina obliquiloculata* (Parker and Jones) is relatively enriched at the top of LU8. The ratio of benthic to planktonic foraminifera shows negligible variations compared to LU9.

LU7 (64.7–54.7 mbsf): The sediments are composed of grey silt interbedded with grey black fine sands, showing fining upward and rhythmic bedding at an interval of 3–40 cm. A small amount of burrows appear in this subunit. However, the sedimentary structures of LU7-2 are heavily bioturbated by the horizontal and vertical burrows. The Mz varies between 4.7 Φ and 6.3 Φ. From bottom to top, the foraminifera abundance reduces with an average of 2000 individuals in 50 g dry sample. In this unit, the planktonic contents decrease obviously, and most are below10%. The dominate benthic species are *Protelphidium tuberculatum*, *Ammonia beccarii* vars. and *Buccella frigida*, and common species are *Nonionella decora*, *Cribrononio incertum*, *Elphidium magellanicum* Heron-Allen and Eerland. Additionally, *Quinqueloculina akneriana rotunda* appears abundantly at the bottom.

LU6 (54.7–46.5 mbsf): It is characterized by grey silt, with heavy bioturbation, very fine molluscan fragments, parallel bedding, lenticular bedding and wave bedding, rhythmic bedding, and lots of burrows in the sediments. Particularly, a fawn muddy nodule is discovered at ca. 54.0 m. The Mz ranges from 3.9 Φ to 5.6 Φ. The abundance of microfossils increases upward, and the main species are *Bolivina robusta*, *Ammonia beccarii* vars., *Nonionella decora*, *Siphouvigerina proboscidea*, *Globocassidulina subglobosa*, *Protelphidium tuberculatum* and *Quinqueloculina akneriana rotunda*. Among which, the percentage of *Bolivina robusta* is more than 5%. The planktonic percentage increases upward from 20% to 80%.

LU5 (46.5–35.9 mbsf): This unit can also be divided into two subunits based on the lithological characters and microfossil

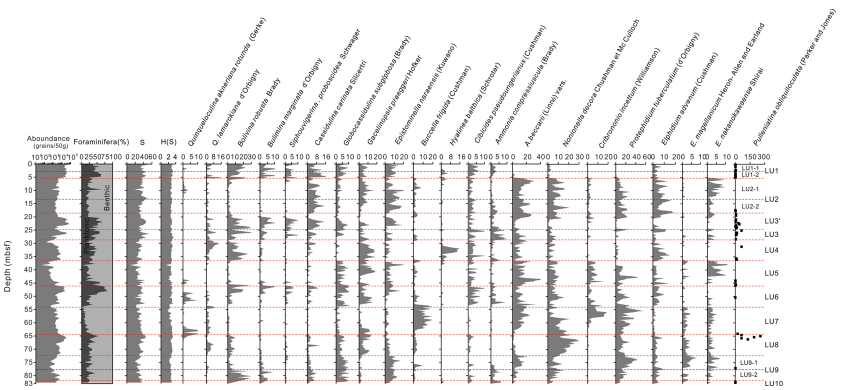

FIGURE 5 | Downcore profiles of foraminifera assemblage in borehole SFK-1. S: simple diversity; H(S): Shannon-Weiner index. H(S)= -ΣPilnPi (Pi refers to proportion of the i-th species). Pulleniatina obliquiloculata (Parker & Jones): numbers of fossils; the other foraminifera: volume percentage.

assemblages. The subunit LU5-1 sediments are mostly black silty sand with a large number of molluscan fragments, while the sediments of LU5-2 are dominated by grey silt interbedded with grey black fine sand, showing subparallel bedding, flaser and lenticular beddings, rhythmic structures, and lots of organic burrows. Moreover, muddy gravels are widely observed in the fine sand layers, being irregular shapes of bar and block. At the bottom, LU5 has an erosional surface.

The grain size parameters including Mz, standard deviation, skewness and kurtosis display remarkable changes in the subunits. The clay contents are all below 10%, while the silt contents are much variable. Microfossils occasionally occur in the unit, with their species numbers (simple diversity) only changing from 22 to 33 individuals in all samples. The benthic foraminifera are dominant, including *Ammonia beccarii* vars., *Protelphidium tuberculatum*, *Nonionella decora*, *Cribrononio incertum*, *Elphidium nakanokawaense* and *Nonion akitaense*, while the abundance of planktonic foraminifera decreases significantly.

LU4 (35.9–27.95 mbsf): It is characterized by gray-black silt, displaying massive bedding, hard texture and occasional flaser bedding. Very fine molluscan fragments and flaser fine sand layers with some dwelling burrows rarely occur in the sediments of 35.9–34.5 mbsf, and an obvious hiatus at its bottom. The silt accounts for 70% and sand content is less than 20%. The microfossil assemblages are dominated by benthic foraminifera, including *Bolivina robusta-Gavelinopsis prageri*, *Ammonia beccarii* vars., *Elphidium advenum*, *Cibicides pseudoungerianus* and *Hyalinea balthica* (Schroter). The content of planktonic foraminifera in LU4 is slightly higher than in LU5.

LU3 (27.95–24.8 mbsf): Three different parts can be recognized in this unit. The upper part is dominated by gray-black sand and grey silt with parallel bedding and lenticular bedding, and high water content at the top. The middle part is composed of medium-fine sands with large pieces of grey clay and molluscan fragments. The lower part is characterized by fawn fine sands mixing with gray black sands and some grey mud gravels, with a clear erosional surface with the overlying subunit. The Mz increases upward and ranges from 5.3 Φ to 3.4 Φ, accompanied with large variations of standard deviation, skewness and kurtosis. The percentage of benthic foraminifera varies upward from 50% to 75%. The main foraminifera are *Ammonia beccarii* vars., *Bolivina robusta*, *Ammonia compressiuscula* (Brady), *Quinqueloculina lamarckiana*, *Cassidulinia carinata* and *Nonionella decora*.

LU3' (24.8–18.2 mbsf): It can be divided into two subunits. The subunit LU3'-1 (20.0–18.2 mbsf) is featured by brownish to gray black silty sands with lots of quartz and mica, and some thin reddish brown oxide layers and ferromanganese nodules occur at 19.2–19.1 mbsf. The subunit LU3'-2 (24.8–20.0 mbsf) mainly consists of fawn fine sands and medium-coarse sands, forming a markedly thick sandy bedding with several thin flaser mud layers and lots of small molluscan fragments. Similarly, quartz and schistose minerals are widely observed in this subunit.

The sediment color of LU3' changes from fawn to gray black upward, with two clear erosion surfaces occurring at each end. The Mz fluctuates between 2.1 Φ to 4.5 Φ, showing a trend of fining upward with large variations of standard deviation, skewness and kurtosis. The coarsest samples appear at the bottom of subunit LU3'-2. The abundance of planktonic foraminifera in LU3' is higher than benthic foraminifera, although their species are relatively few. The dominated benthic species are *Ammonia beccarii* vars., *Bolivina robusta* and *Protelphidium tuberculatum*. While, *Cassidulinia carinata*, *Elphidium advenum*, *Nonionella decora*, *Buccella frigida* and *Cribrononion incertum* are also widely observed. A striking peak of planktonic foraminifera with small shells occurs at the lower part of the unit.

LU2 (18.2–5.2 mbsf): The flaser bedding, lenticular bedding, wavy bedding and some parallel bedding are well developed in this unit that is dominated by the interbedded gray-black sand and gray silt. The two sub-units, LU2-1 and LU2-2, show different grain size compositions but both with fining bottom-up. A large number of gray mud gravels of irregular shapes are found at the bottom of the unit, with few shell fragments. The Mz ranges at 3.0–6.0 Φ, showing coarsening to fining and then coarsening trends upward. The ratio of the benthic to planktonic foraminifera is relatively stable, completely different from that in LU3. The

dominant fossil assemblage is *Ammonia beccarii* vars.- *Protelphidium tuberculatum* (d'Orbigny)- *Episominella naraensis*, occupying over 30% of the total abundance. The species with the percentages between 5% and 10% include *Elphidium advenum*, *Elphidium nakanokawaense* Shirai and *Nonionella decora* (Cushman et Mc Culloch). In addition, *Buccella frigida* (Cushman), *Cribrononio incertum* (Williamson), *Quinqueloculina akneriana rotunda* (Gerke) and *Quinqueloculina lamarckiana* (d'Orbigny) are also common in the samples.

LU1 (5.2–0 mbsf): Two subunits comprise this top unit, among which one is composed of gray-black silty sand (LU1-1, 2.80–0 mbsf, **Figures 3**, **4**), and another characterized by dark grey medium-fine sand (LU1-2, 5.2–2.8 mbsf). A distinct erosional surface exits between these two subunits. LU1-1 is mixed with flaser grey silt layers and plentiful shell fragments with a high water content. LU1-2 is well sorted, mixed with some shell fragment layers, rich in quartz, with an erosional contact with the underlying layer. The sand content of LU1-1 decreases from 79% to 36% upward, while the coarsest sediments of the whole borehole appear in the LU1-2 with the sand contents higher than 94%. In addition, the fossil abundance reaches high numbers of 7352–79960 individuals per 50 g dry sample, with the peak number appearing at the surface sediments. The characteristic species are *Bolivina robusta* (Brady), *Epistominella naraensis* (Kuwano), *Cassidulinia carinata* (Silcertri), *Globocassidulina subglobosa* (Brady), *Siphouvigerina proboscidea* (Schwager) and *Hanzawaia nipponica*. The abundance of planktonic foraminifera in LU1-1 is much higher than in LU1-2, with *Ammonia beccarii* vars. (Linné) being absent in LU1-1 but occasionally observed in LU1-2.

4.3 OSL and Radiocarbon Ages of Core SFK-1

For ages by both radiocarbon and OSL dating, most of them occur in stratigraphic order in the core (**Tables 1**, **2**), and agree with each other. The OSL ages demonstrate a reasonable chronological framework up to ca. 100 ka (**Figure 6**). The radiocarbon ages were measured on benthic foraminifera and molluscan shells, respectively, which might be overestimated for their re-deposition under strong hydrodynamic environments, i.e. in fluvial and nearshore sedimentation (Xu et al., 2020). Contamination by younger carbon can lead to biased younger ages (Pigati et al., 2007; Lai et al., 2014; Song et al., 2015). Therefore, the radiocarbon ages are used as supplementary supporting data in the age model, and those in apparent disorder were not included in the age model (**Figure 6**).

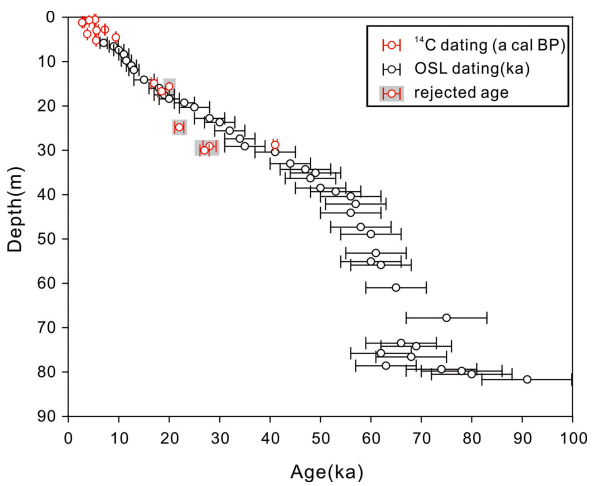

FIGURE 6 | Age model of SFK-1 on the basis of OSL and ^{14}C dates.

4.4 Sedimentary Facies and Stratigraphic Framework of Core SFK-1

Based on the above mentioned sediment characters, foraminifera assemblages and dating results, the stratigraphic framework and sedimentary facies of core SFK-1 from the outer shelf of ECS are reconstructed (**Figure 7**). In summary, the late Quaternary deposition from bottom to top is characterized by neritic and prodelta facies in mid MIS 5, tidal sand ridge and littoral-tidal flat facies in late MIS 5, estuarine-tidal flat and tidal nearshore facies in MIS 4, neritic facies in early MIS 3, nearshore facies in late MIS 3, tide-influenced fluvial and estuarine facies in LGM, tidal flat facies in late MIS 2, and tidal sand ridge facies in the Holocene (MIS 1).

Neritic and prodelta facies during the mid MIS 5 (corresponding to LU9, SU9): They are characterized by gray silt with massive bedding. The lower neritic facies gradually changes to the upper prodelta deposition without an obvious hiatus. The foraminifera assemblage is dominated by the mid-shelf species of *Bolivina robusta* and *Globocassidulina subglobosa*, while the warm-water species of *Cibicides pseudoungerianus* and *Hyalinea balthica* reduce upward in abundance and the cold water species increase, respectively. Additionally, the nearshore shallow water species of *Protelphidium tuberculatum* and *Ammonia beccarii* vars. and some burrows appear and gradually increase. The relatively high ratio of planktonic to benthic microfossil in LU9 also indicates that they are in a neritic sedimentary environment (**Figure 5**). These observations and dating results suggest that the sedimentary facies probably developed during the MIS 5c–5b at about 100 ka, with the sea level probably declining gradually from the high stand (Wang et al., 1985; Wang et al., 1988).

Tidal sand ridge facies during early transgression in late MIS 5 (LU8, SU8): The remarkable feature of this facies is high sand content with positively biased skewness and massive bedding, which indicates a stronger hydrodynamic depositional environment and/or proximal provenance. The microfossil assemblages show a striking reduction of shallow water species, the disappearance of typical euryhaline brackish species of *Ammonia beccarii* vars., and a relatively low content of deep water species of *Bolivina robusta* (Wang et al., 1985; Yang et al., 1998; Liu et al., 2010). This microfossil assemblage indicates the MIS 5a deposition was formed at the water depth of 30–50 m (Wang et al., 1985). Moreover, the high content of cold water species *Protelphidium tuberculatum* and *Buccella frigida* might result from the intrusion of cold current or weak warm current (Wang et al., 1988; Li et al., 2014b; Mei et al., 2016). The OSL

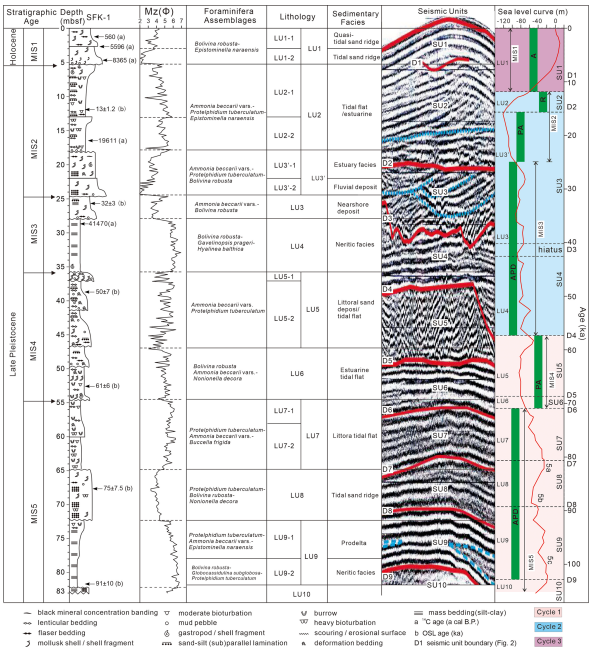

FIGURE 7 | Correlation of SFK-1lithologic units with grain size and foraminifera assemblages, seismic units and the global sea level curve. LU and SU indicates depositional units and seismic units, respectively, and D denotes the discontinuity or depositional hiatus. The sea level curve is modified from Chappell et al. (2002). Cycles 1-3 refers to the cycle of marine transgression and regression sequences. APD, PA and R indicates the stratigraphic motif of aggradation- progradation-degradation, aggradation- progradation, retrogradation proposed by Neal and Abreu (2009).

dates indicate this depositional unit was formed at about 80 ka (**Figures 6**, **7**). It can be inferred that the deposits might be formed on mid-shelf dominated by the strong tide current and early marine transgression of MIS 5a.

Littoral-tidal flat facies in late MIS 5 (LU7 and SU7) and estuarine-tidal flat facies of MIS 4 (LU6 and SU6): These depositional units are characterized by rhythmic mud- sand alternations of gray black fine sand, weakening bioturbation, normal graded bedding sequence, and gradually better sorting upward. Deep water species of *Gavelinopsis prageri* and *Sigmoilopsis asperula* and small shells of planktonic foraminifera in LU7 are widely observed whose contents are significantly lower than that in both LU8 and LU9, while shallow water species of *Ammonia beccarii* vars. and *Cribrononion incertum* only occur at the bottom (**Figure 7**). All the above observations of LU7 clearly indicate that it developed under a nearshore environment, forming littoral-tidal flat deposits on the inner shelf. The depositional environment of LU6 is similar to LU8, except for higher abundance of planktonic foraminifera. The sudden increase of deep water benthic foraminifera of *Bolivina robusta*, *Siphouvigerina proboscidea* and *Globocassidulina subglobosa* indicates some fluctuation of sea level.

The evidences of sediment coarsening upward, large numbers of shell fragments, more bioturbation, and a few of yellow-brown mud gravels, all indicate the estuarine and/or tidal flat facies of LU6. Two seismic facies (SU6 and SU7) correspond well with the two sedimentary facies (LU6 and LU7), and both are characterized by subparallel and continuous reflections, medium amplitudes, onlap of NE direction. These features indicate a typical progradation in forced regressive systems tract (FRST) (Catuneanu, 2002). Based on the OSL ages and eustatic sea level change during MIS 5a, we interpret these two depositional units as the littoral-tidal flat and estuarine-tidal flat facies developed at 70–80 ka (**Figure 6**).

Tidal nearshore facies during the MIS 4 (LU5; SU5): The sediments are identified as typical tidal deposition, showing grey to gray black lenticular and flaser bedding, higher bioturbation intensity (numerous burrows), and distinctive black shell sand at the top. Microfossil assemblages suggest an environment of cold water and low salinity at the depth of 20 m below sea surface. The number of cold species of benthic foraminifera including *Protelphidium tuberculatum*, *Buccella frigida* and *Elphidium magellanicum* suddenly increased, while the planktonic foraminifera reduced in abundance (**Figure 5**), indicating shallower water (Wang et al., 1985; Wang et al., 1988). The age of this unit is inferred at ca. 55–68 ka (**Figure 6**).

Neritic facies in the MIS 3 (LU4; SU4): It is featured by homogeneous gray black silt with massive bedding, no obvious bioturbation, and typical shallow sea species of *Bolivina robust* and warm species of *Cibicides pseudoungerianus* and *Hyalinea balthica*. These observations indicate a neritic and warm water condition (Wang et al., 1988). One AMS ^{14}C age of benthic foraminifera is 41470 a cal B.P. at 28.8 mbsf, suggesting the sedimentation in MIS 3 (**Figures 6**, **7**).

Nearshore facies of late regression in early MIS 2/late MIS 3 (LU3; lower SU3): It is dominated by parallel bedding with some

lenticular bedding, forming two erosion surfaces at the top and bottom. A transitional or coastal shelf sedimentary environment is indicated by the coexistence of typical euryhaline brackish species of *Ammonia beccarii* vars. and the representative shallow water species in the middle shelf of *Bolivina robusta* (Wang et al., 1985). The deposition might partly develop during the late MIS 3 (**Table 1** and **Figure 6**).

Fluvial and estuarine facies during the LGM (LU3'; upper SU3): It is characterized by a normal graded vertical sequence with the dominance of yellow brown–grey sorted sands. Both planktonic and benthic foraminifera reach their peak abundances in this depositional unit, and most of them are a mass of very small and re-worked planktonic foraminifera, transported by the currents after previous deposition and mixed with larger and intact bodies of nearshore euryhaline brackish species of benthic foraminifera and abundant cold species. The microfossil observation as well as the dating results suggest that this unit was tidal river and estuarine sedimentation in the LGM.

Tidal flat facies during the deglaciation of late MIS 2 (LU2; SU2): The striking feature of this unit is tidal flat with sand and mud interstratification, and flaser, lenticular and little parallel beddings. The depositional ages were confined to the late MIS 2 based on the OSL dates (**Table 2** and **Figure 6**). Due to the sea level fluctuation during the deglacial period, two different depositional subunits formed, corresponding to the two stages of slow sea level rise, while the hiatus between them apparently coincides with the melt-water pulses (MWP-1A, 14.5–13.7 ka) in the last transgression on the ECS shelf (Fairbanks, 1989; Bard et al., 1990; Liu and Milliman, 2004a; Li et al., 2005b). The dominance of nearshore species *Ammonia beccarii* vars. and cold species *Protelphidium tuberculatum* reveals a depositional environment of euryhaline brackish and cold water, with a relative sea level rise from the lowest stand (Chappell et al., 1996).

Tidal sand ridge facies in the Holocene (LU1; SU1): A typical assemblage of *Bolivina robusta* suggests a mid-outer shelf environment (Wang et al., 1985; Wang et al., 1988), although two different parts can be distinctly identified by sediment grain size composition. The upper one is mainly composed of silt and clay, with occasional thin flaser muddy layers occurring in the massive black sandy deposits, which are defined as quasi–active tidal sand ridges mixed with modern fine sediments (Liu et al., 2007a). Their ages are dated at 560 a cal B.P. at 1.2 mbsf and 5596 a cal B.P. at 2.80 mbsf, respectively (**Table 1**), diagnostic of the mixed sedimentation. The lower part is characterized by well-sorted sandy sediments. The dominant microfossil group of *Ammonia beccarii* vars. and *Protelphidium tuberculatum* at the bottom presents an eurythermal and euryhaline environment, when the tidal sand ridge began to develop in the early Holocene. Low value of *Pulleniatina obliquiloculata* coincides with the *P. obliquiloculata* Minimum Event (PME) during the Holocene (Lin and Hsieh, 2007).

5 DISCUSSIONS

5.1 Evolution of Sedimentary Environment on the Outer Shelf of ECS Since MIS 5

The basic features of seismic reflections on the profile A-B across SFK-1 are overall similar with previous studies (**Figure 2**). For example, the reflection boundary D3 in this study corresponds to the top boundary of U2b defined by Yang (1989), the boundary D130 in Berné et al. (2002), the boundary SB1 in Wellner and Bartek (2003), the boundary QR2 in Li et al. (2005a), and the boundary T3 in Xu et al. (2020), respectively. Additionally, seismic unit SU5 coincides well with U110 in Berné et al. (2002), U7 in Liu et al. (2000), and SU5 in Xu et al. (2020) (**Table 3**). Nevertheless, the consensus on regional stratigraphic framework of the ECS shelf has never been reached in these previous studies mainly because of the absence of high-resolution depositional ages on drilling boreholes (Yang, 1989; Tang, 1996; Saito et al., 1998b; Liu et al., 2000; Berné et al., 2002; Yang, 2002; Yoo et al., 2002; Wellner and Bartek, 2003; Wu et al., 2010; Xu et al., 2020). In particular, it is still an open question on the recognition and interpretation of MIS 6 strata in the seismic stratigraphy by Liu et al. (2000), Berné et al. (2002) and Xu et al. (2020) (**Table 3**).

By comparing the sedimentary facies (**Figure 7**), seismic reflection facies of profile across boreholes SFK-1 and DZQ4

TABLE 3 | Comparison in the interpretation of seismic stratigraphy on the ECS outer shelf between previous studies and this work.

Liu et al., 1999; Liu et al., 2000; Wu et al., 2010		Berné et al., 2002		Xu et al., 2020		This study	
Seismic Unit	**Marine Isotopic Stage**	**Seismic Unit**	**Maine Isotopic Stage**	**Seismic Unit**	**Maine Isotopic Stage**	**Seismic Unit**	**Maine Isotopic Stage**
U2	MIS 1	U140b	MIS 1	SU1	MIS 1	SU1	MIS 1
U3	MIS 3.1	U140a					
U4	MIS 3.2	U130	MIS 2	SU2		SU2	MIS 2
				SU3		SU3	
U5	MIS 3.3	U125	MIS 5.2-3	SU4	MIS 5.5-3	SU4	MIS 3
U6	MIS 5.1	U120	MIS 5.3-5.5				
U7	MIS 6	U110	MIS 6	SU5	MIS 6-MIS 5.5	SU5	MIS 4
		U90	MIS 7	SU6	MIS 7-6	SU6	MIS 5
		U80?				SU7	
		U70				SU8	
		U60		SU7	MIS 8-7	SU9	
		U55	MIS 8	SU8	MIS 8	SU10?	MIS 6?

(**Figure 2**), and global sea level curve (**Figure 7**) (Chappell et al., 1996), we recognize almost three cycles of marine transgression and regression sequences (Cycle 1 to Cycle 3, hereafter) that comprise continuous deposition without major stratum hiatus on the outer shelf of ECS since the mid-MIS 5 (**Figure 7**). These cycles in sedimentary records can be well compared with eustatic sea-level highstands at 105–97, 88–80, 60, 50–40 and 30–28 ka, apparently matching with the Milancovitch precessional (20 kyr) cycles (Lobo and Ridente, 2014). A scenario of the late Quaternary sedimentation on the outer shelf of ECS is clarified by using the sequence stratigraphy hierarchy from Neal and Abreu (2009) (**Figure 7**).

5.1.1 Aggradation- Progradation- Degradation (APD) Processes of Cycle 1 in MIS 5

This last interglacial period MIS 5 is regarded as the highstand stage of a cycle with relatively slight sea level fluctuation (Chappell and Veeh, 1978; Siddall et al., 2003; Lobo and Ridente, 2014). Both the seismic reflection interpretation and core SFK-1 records suggest the neritic deposition in MIS 5c, and the warm water species indicate warm currents at that time, forming the aggradation of APD (Wang et al., 1987; Ujiie et al., 2003; Lin and Hsieh, 2007; Neal and Abreu, 2009; Liu et al., 2011). With the slight fall of seal level during MIS 5b (Chappell, 2002; Culter et al., 2003), the prodelta progradation happened without obvious hiatus on the outer shelf. Correspondingly, the abundance of warm water species reduced while the euryhaline brackish species increased, which probably suggest the increasing input of fluvial water or the intrusion of cold water mass under a favorable summer monsoon climate during the interglacial period (Cheng et al., 2016; Dai et al., 2021).

After that, the tidal sand ridge began to develop in response to the strong tidal current system of Pacific with decelerated sea level rise and coastal accommodation, forming the degradation of APD (**Figure 7**) (Liu et al., 2003, Liu et al., 2007a; Neal and Abreu, 2009). The strong tide current might erode and re-distribute the former fine prodelta deposits, and gradually formed coarser sandy sedimentation. An apparent erosional surface existed between the tidal sand ridge deposition and the overlying prodelta deposition in the study area. Those buried sand ridges distributed locally on the mid-outer shelf of ECS.

In theory, the Maximum Flooding Surface (MFS) will form with the depositional environment changing from retrogradation to progradation. The MFS deposits appeared in the MIS 5a on ECS shelf, evidenced by high contents of silt and clay (>55%) and maximum foraminifera abundance with rhythmic bedding and upward-fining trend. The typical warm species of planktonic foraminifera accustomed to live at the water depth of 50–100 m, *Pulleniatina obliquiloculata* (Parker & Jones) suddenly abounded in MIS 5a (Wang et al., 1987; Liu et al., 2011). Meanwhile, a number of heavily-worn cold water species, which might come from the former sediments of MIS 5c-MIS 5b by erosion and re-accumulation process in regression. With the increasing influence of tidal current in quick regression of late MIS 5a, the wide nearshore tidal flats deposited on the mid-outer shelf, and formed one part of APD (**Figure 7**). Correspondingly, the dominant foraminifera switched from deep water species of mid-outer shelf to nearshore shallow water species.

5.1.2 Progradation- Aggradation (PA) Processes of Cycle 1 in MIS 4

Estuarine tidal flats developed in early MIS 4 following the continuous sea level fall. More bioturbation and occasional yellow-brown mud gravel characterized the estuarine tidal flat deposition under much shallower seawater based on the global sea level record (**Figure 7**, Chappell, 2002). In later MIS 4, the sea level fluctuated significantly in response to the glacier change, rising from 90 m below present one to 70 m within a short period (Martinson et al., 1987). The frequent sea level changes might rework the former deposits and resulted in the deposition of nearshore tidal flat and black shell sands in response to quick transgression, forming several PA successions as observed in SFK-1 (**Figure 7**). In that period, cold species foraminifera *Protelphidium tuberculatum* widely occupied the outer shelf of ECS. It is noteworthy that the deposits were previously identified as the MIS 6 strata with the evidences from seismic stratigraphy (Liu et al., 2000; Berné et al., 2002; Wu et al., 2010; Xu et al., 2020) (**Table 3**). Although the MIS 4 and MIS 6 periods might share similar sea levels and climate regimes, our combined data from seismic profiling observations and high-resolution core records with robust chronostratigraphic constraints, suggest it could be regarded as the MIS 4 strata. Additionally, the frequent sea level fluctuation with relatively small amplitudes caused no transgression deposits in the successions.

5.1.3 Aggradation- Progradation- Degradation (APD) Processes of Cycle 2 in MIS 3

Relatively weak variability in sea level happened during MIS 3 (25–60 ka), fluctuating from 90 m to 60 m below present one (Chappell et al., 1996; Chappell, 2002; Waelbroeck et al., 2002; Siddall et al., 2008). On the ECS shelf, a wide neritic deposition of aggradation and progradation happened with the slow decline of sea level, displaying the strong, continuous and lateral progradational configuration on the seismic profile. The relatively warmer climate in early MIS3 (Zhen et al., 2008) led to more warm species inhabiting in water of 50 m deep. The sediment accumulation rate was low due to the far distance to the continent with relatively high sea-level. At ca. 40 ka in middle MIS 3, a glaciation was caused by the low solar radiation of low and middle latitude in summer due to the effect of precession, which led to a quick sea level fall and most of shelf exposed in a short time (Cheng et al., 2016). Therefore, a sedimentation hiatus formed between the progradation and degradation (**Figure 7**) (Marsset et al., 1996; Liu et al., 1999; Liu et al., 2000; Li et al., 2002a; Neal and Abreu, 2009; Xu et al., 2018), which were also observed on the shelves of Yellow Sea and Bohai Sea (Yang et al., 1996; Marsset et al., 1996). The marine-continental transitional facies of sand and mud interstratifications developed under the sea level fluctuation caused by multiple Heinrich and Dansgaasid-Oeschger incidents of millennial scales in late MIS 3. In addition, the costal line continuously retreated seaward on the whole in response to the drop of sea level (Jouzel et al., 1987; Dansgaard et al., 1993; Grootes et al., 1993; Zhao et al., 2008).

5.1.4 Progradation- Aggradation (PA) and Retrogradation (R) Processes of Cycle 2 in MIS 2

During the LGM (18–22 ka), the fluvial, nearshore estuary and costal deposition formed due to the gentle topography of the ECS shelf, with drastic fluvial incision and sea level drop, which corresponds to the PA deposit (**Figure 7**).

As introduced above, whether the deposits such as MIS 2 and 4 can be preserved and recognized on the dynamic shelf environment is still controversial. During the glacial periods with extremely low sea level, the rivers mostly bypassed the exposed continental shelf, without accumulating thick sediments because of limited accommodation space (**Figure 7**) (Liu et al., 1999; Liu et al., 2000; Liu et al., 2003; Wu et al., 2010; Xu et al., 2018). While the others suggest that the deposition could be still well preserved and recognized on the open shelf during sea level lowstands (Berné et al., 2002; Li et al., 2002a; Yu et al., 2006; Wang et al., 2013; Wang et al., 2014). Our observations clearly indicate the occurrence of deposition during the last glacial period on the ECS outer shelf (**Figure 7**), based on the high-resolution seismic profiles and core records, as well as robust chronostratigraphic constraints of OSL and AMS ^{14}C dates (**Figure 6**).

The sedimentary characters and microfossil assemblages suggest that the fluvial sediments on the outer ECS shelf were strongly influenced by the tide-wave system from the west Pacific in the estuary and lower reaches (Liu et al., 2007a). Because the costal lines migrated towards the outer shelf close to the Okinawa Trough, plenty of very small and heavily broken or reworked planktonic larvae fossils accumulated in the tide-influenced area and tidal estuary (Wang et al., 1985; Liu et al., 2003; Liu et al., 2007a; Zhao et al., 2008; Wang et al., 2013). With the paleoclimate becoming colder in MIS 2, less terrigenous material was transported into the sea by rivers, and meanwhile, the depositional environment witnessed a remarkable change from fluvial to tidal dominance (Winkler and Wang, 1993; Wellner and Bartek, 2003; Liu et al., 2007a; Wang et al., 2013; Wang et al., 2014). Though multiple cycles of estuary and fluvial deposition can be identified on some seismic profiles (for example, **Figure 2**, SU3-1~SU3-3) (Yang, 1989; Saito et al., 1998b; Chen et al., 2000; Liu et al., 2000; Berné et al., 2002; Li et al., 2002a; Wellner and Bartek, 2003; Wang et al., 2013), these fluvial and estuarine deposits are generally very thin and were poorly preserved on the mid-outer shelf, and thus are hardly recognized on seismic profiles (Saito et al., 1998b; Liu et al., 2000; Zhao et al., 2008; Xu et al., 2018; Xu et al., 2020).

During the early deglacial transgression (late MIS 2) with the global climate warming and ice sheet melting (**Figure 7**), the paleo-river mouth and coastal line retreated landward in response to sea level rise (Saito, 1998a; Liu et al., 2000; Wellner and Bartek, 2003; Li et al., 2005b; Xu et al., 2018; Xu et al., 2019). Correspondingly, the incised valleys were first filled and the estuarine and tidal-flat facies formed, as reported in previous studies (Allen, 1991; Woodroffe et al., 1993; Dalrymple and Zaitlin, 1994). The tidal current became stronger following the rapid sea level rise, which resulted in the wide tidal flats developing on the gentle shelf of ECS. The nearshore sediments accumulated at the LGM were eroded, transported and re-distributed, and finally formed the tidal deposition (Dalrymple et al., 1992; Berné et al., 2002; Yang, 2002; Wang et al., 2014). Melt-water Pulses 1A and 1B (Fairbanks, 1989; Bard et al., 1990) during this period probably resulted in two hiatuses with the rapid rise of sea level (Liu et al., 2004b; Li et al., 2014a), changed sedimentary environment and caused shelf erosion. However, the tidal deposits corresponding to the early TST could develop retrogradation during the period of slow sea level rise (**Figure 7**) (Uehara et al., 2002; Uehara and Saito, 2003).

5.1.5 Aggradation of APD Process of Cycle 3 in Holocene

At the beginning of the Holocene, the sea level was at about 50 m below present one, and then reached the highest at 7 ka (Zhu et al., 1979; Chen et al., 1985; Saito, 1998a). The whole outer shelf of ECS was affected by the strong tidal current, and correspondingly, the transgressional tidal sand ridges that consist of well sorted black gray medium sands formed. Whereas, the tidal current and ocean current might be still powerful after sea level rising to the highest, which was verified by the measured value of Acoustic Doppler Current Profiling (ADCP) during borehole SFK-1 drilling. The flow velocity of sea bottom current can reach 0.13 cm/s in a tide cycle under the good sea condition (Su et al., 2008). A current velocity of 0.55 cm/s was once reported in previous study (Berné et al., 2002), and the velocity of 60–70 cm/s was calculated and inferred to be reasonable under the spring tide and stormy conditions (Liu and Milliman, 2004a; Liu et al., 2010). Therefore, the former sediments deposited during the last transgression could be eroded and redistributed, forming an obvious erosional surface, while simultaneously few modern suspended load carried by sea current might accumulate and mix with the eroded shelf sediments, forming the quasi-active sand ridge (**Figure 7**). This has been recognized as one striking feature of aggradation deposition of APD process in the ECS (Liu et al., 2007a; Xu et al., 2018).

6 CONCLUSIONS

In combination with the high-resolution seismic interpretation, the integrated study of chronostratigraphy, biostratigraphy and sedimentary facies of borehole SFK-1 reveals almost three cycles of relatively continuous transgression- regression sequences developed on the outer shelf of ECS since MIS 5. The stratigraphic boundaries between MIS 2 and MIS 3, and between MIS 4 and MIS 5, are identified to be the erosional surfaces between fluvial and marine transgressive deposits, and between estuarine tidal flat and nearshore tidal flat deposits, respectively. These hiatuses can easily be recognized in the sediment facies, however cannot be identified in seismic profile interpretation mainly because of the relatively continuous reflection. The two staircases of lowstand of sea level during the last glaciation, i.e. early glacial staircase in MIS 4 and late one during the LGM were well preserved on the shelf strata, which can be treated as two marker layers for correlation of late Quaternary strata on the outer shelf of the ECS. Late Quaternary marine transgression generally resulted in the formation of tidal deposition on the ECS shelf, which is characterized by distinct reverse graded bedding. This observation

is different from the general understanding that marine transgression tends to form the normal graded bedding. The major reason for the different observations probably lies in the widespread and strong tidal influence on the ECS shelf in response to rapid sea level rise.

Due to the gentle topography of the open shelf, the sediment transportation patterns switched from seaward to landward during marine transgression, and thus the previously deposited sediments were eroded, redistributed and transported landward by tidal current, forming the coarsening deposits upward. In comparison, the delta and/or tidal flat facies developed in different stages of marine regression. In brief, tidal deposition is the most striking feature on the late Quaternary stratigraphy of the open ECS shelf. Our study also revealed that the outer shelf of ECS was not completely exposed to be land during the low sea level stages of MIS 4 and MIS 2, but subjected to strong tidal influence, which consequently preserved the tide-influenced fluvial, estuarine and tidal flat deposition on the open shelf. The sedimentary stratigraphic evolution together with the shifts of major depocenters on the ECS shelf during the late Quaternary suggest the complex river-sea interaction and the first-order control of sea level changes on the siliciclastic shelf deposition.

DATA AVAILABILITY STATEMENT

The original contributions presented in the study are included in the article/supplementary material. Further inquiries can be directed to the corresponding author.

AUTHOR CONTRIBUTIONS

ZW: Conceptualization, Methodology, Software, Formal analysis, Writing - Original Draft. SY: Conceptualization, Supervision, Writing – review & editing. HT, YLZ, and HW: Data Curation. ZH: Resources, Project administration, Review. YZ and XM: Writing – review & editing. QW: Supervision, LZ: Supervision and Revision. Review. All authors contributed to the article and approved the submitted version.

FUNDING

This research was jointly funded by National Natural Science Foundation of China (Grant Nos. 41876059, 41730531, 41991324 and 42176078), China Geological Survey (Grant Nos. DD20190377, DD20190208, DD20190236, DD20221710 and DD20160137), and Shantou University Scientific Research Foundation (Grant No. NTF20028).

ACKNOWLEDGMENTS

We express our gratitude to the crew of D/V Kan 407 in acquiring the geological core. We thank Congxian Li, Zhengxia Liu, Qixiang He and Zigeng Yang for their insightful comments and suggestions during the manuscript preparation. We are grateful to Hemao Lin, Xixian He, Hong Wang and Zhaokai Xu for the microfossil identification.

REFERENCES

Allen, G. P. (1991). "Sedimentary Processes and Facies in the Gironde Estuary: A Recent Model for Macrotidal Estuarine Systems," in *Clastic Tidal Sedimentary, Clastic Tidal Sedimentary. Canadian Society of Petroleum Geologists Memoir*, vol. 16 . Eds. D. G. Smith, G. E. Reinson, B. A. Zaitlin and R. A. Rahmani, 29–40.

Bard, E., Hamelin, B., Fairbanks, R. G., and Zindler, A. (1990). Calibration of the 14-C Timescale Over the Past 30,000 Years Using Mass Spectrometric U-Th Ages From Barbados Corals. *Nature* 345, 405–409. doi: 10.1038/345405a0

Berné, S., Vagner, P., Guichard, F., Lericolais, G., Liu, Z. X., Trentesaux, A., et al. (2002). Pleistocene Forced Regressions and Tidal Sand Ridges in the East China Sea. *Mar. Geol.* 188 (3–4), 293–315. doi: 10.1016/S0025-3227(02)00446-2

Bi, L., Yang, S. Y., Zhao, Y., Wang, Z. B., Dou, Y. G., Li, C., et al. (2017). Provenance Study of the Holocene Sediments in the Changjiang (Yangtze River) Estuary and Inner Shelf of the East China Sea. *Quat. Int.* 441 (Part A), 147–161. doi: 10.1016/j.quaint.2016.12.004

Catuneanu, O. (2002). Sequence Stratigraphy of Clastic systems: Concepts, Merits, and Pitfalls. *J. Am. Earth Sci.* 35, 1-43. doi: 10.1016/S0899-5362(02)00004-0

Chappell, J. (2002). Sea Level Changes Forced Ice Breakouts in the Last Glacial Cycle: New Results From Coral Terraces, Quat. *Sci. Rev.* 21 (10), 1229–1240. doi: 10.1016/S0277-3791(01)00141-X

Chappell, J., Omura, A., Esat, T., McCulloch, M., Pandolfi, J., and Pillans, B. (1996). Reconciliation of Late Quaternary Sea Levels Derived From Coral Terraces at Huon Peninsula With Deep Sea Oxygen Isotope Records. *Earth Planet. Sci. Lett.* 141, 227–236. doi: 10.1016/0012-821X(96)00062-3

Chappell, J., and Veeh, H. H. (1978). $^{230}Th/^{234}U$ Age Support of an Interstadial Sea Level of -40 m at 30,000 yr BP. *Nature* 276 (5688), 602–604. doi: 10.1038/276602a0

Cheng, H., Edwards, R. L., Sinha, A., Spötl, C., Yi, L., Chen, S., et al. (2016). The Asian Monsoon Over the Past 640,000 Years and Ice Age Terminations. *Nature* 534, 640e646. doi: 10.1038/nature18591

Chen, Y. J., Peng, G., and Jiao, W. J. (1985). Radiocarbon Dates From the East China Sea and Their Geological Implications. *Quat. Res.* 24, 197–203. doi: 10.1016/0033-5894(85)90006-7

Chen, Z. Y., Song, B. P., Wang, Z. H., and Cai, Y. L. (2000). Late Quaternary Evolution of the Sub-Aqueous Yangtze Delta, China: Sedimentation, Stratigraphy, Palynology, and Deformation. *Mar. Geol.* 162, 423–441. doi: 10.1016/S0025-3227(99)00064-X

Cong, J. Y., Zhang, Y., Hu, G., Mi, B. B., Kong, X. H., Xue, B. Y., et al. (2021). Textures, Provenances, and Transport Patterns of Sediment on the Inner Shelf of the East China Sea. *Cont. Shelf Res.* 232, 104624. doi: 10.1016/j.csr.2021.104624

Culter, K. B., Edwards, R. L., Taylor, F. W., Cheng, H., Adikins, J., Gallup, C. D., et al. (2003). Rapid Sea-Level Fall and Deep-Ocean Temperature Changes Since the Interglacial Period. *Earth Planet. Sci. Lett.* 206 (3–4), 253–271. doi: 10.1016/S0012-821X(02)01107-X

Dai, L., Li, S., Yu, J., Wang, J., Peng, B., Wu, B., et al. (2021). Palynological Evidence Indicates the Paleoclimate Evolution in Southeast China Since Late Marine Isotope Stage 5. *Quat. Sci. Rev.* 266, 106964. doi: 10.1016/j.quascirev.2021.106964

Dalrymple, R. W., and Zaitlin, B. A. (1994). High-Resolution Sequence Stratigraphy of a Complex, Incised Valley Succession, Cobequid Bay-Salmon River Estuary, Bay of Fundy, Canada. *Sedimentology* 41, 577–612. doi: 10.1111/j.1365-3091.1994.tb01442.x

Dalrymple, R. W., Zaitlin, B. A., and Boyd, R. A. (1992). A Conceptual Model of Estuarine Sedimentation. *J. Sediment. Petrol.* 62, 1130–1146. doi: 10.1306/D4267A69-2B26-11D7-8648000102C1865D

Dansgaard, W., Johnse, S. J., Clausen, H. B., Jensen, D. D., Gundestrup, N. S., Hammer, C. U., et al. (1993). Evidence for General Instability of Past Climate From a 250-Kyr Ice-Core Record. *Nature* 364, 218–220. doi: 10.1038/364218a0

Duller, G. A. T. (2003). Distinguishing Quartz and Feldspar in Single Grain Luminescence Measurements. *Radiat. Meas.* 37, 161–165. doi: 10.1016/S1350-4487(02)00170-1

Emery, K. O., Niino, H., and Sullivan, B. (1971). "Post-Pleistocene Levels of the East China Sea," in *Late Cenozoic Glacial Ages*. Ed. K. K. Turekian (New Haven: Yale University Press), 381–390.

Fairbanks, R. G. (1989). A 17000-Year Glacio-Eustatic Sea Level Record: Influence of Glacial Melting Rates on the Younger Dryas Event and Deep-Ocean Circulation. *Nature* 342, 637–642. doi: 10.1038/342637a0

Folk, R. L., and Ward, W. C. (1957). Barazos River Bar: A Study in the Significance of Grain Parameters. *J. Sediment. Res.* 31, 514–519. doi: 10.1306/74D70646-2B21-11D7-8648000102C1865D

Gao, S., and Collins, M. B. (2014). Holocene Sedimentary Systems on Continental Shelves. *Mar. Geol.* 352, 268–294. doi: 10.1016/j.margeo.2014.03.021

Grootes, P. M., Stuiver, M., White, J. W. C., Johnsen, S., and Jouzel, J. (1993). Comparison of Oxygen Isotope Records From GISP2 and GRIP Greenland Ice Cores. *Nature* 366, 552. doi: 10.1038/366552a0

Heaton, T. J., Köhler, P., Butzin, M., Bard, E., Reimer, R. W., Austin, W. E., et al. (2020). Marine20-The Marine Radiocarbon Age Calibration Curve (0–55,000 Cal BP). *Radiocarbon.* 62, 779–820. doi: 10.1017/RDC.2020.68

Hori, K., Saito, Y., Zhao, Q. H., and Wang, P. X. (2002). Architecture and Evolution of the Tide-Dominated Changjiang (Yangtze) River Delta, China. *Sediment Geol.* 146, 249–264. doi: 10.1016/S0037-0738(01)00122-1

Jouzel, J., Lorius, C., Petit, J. R., Genthon, C., Barkov, N. I., Kotlyakov, V. M., et al. (1987). Vostok Ice Core: A Continuous Isotope Temperature Record Over the Last Climatic Cycle (160,000 Years). *Nature* 329, 403–408. doi: 10.1038/329403a0

Lai, Z. P. (2010). Chronology and the Upper Dating Limit for Loess Samples From Luochuan Section in Chinese Loess Plateau Using Quartz OSL SAR Protocol. *J. Asian Earth Sci.* 37, 176–185. doi: 10.1016/j.jseaes.2009.08.003

Lai, Z. P., Mischke, S., and Madsen, D. (2014). Paleoenvironmental Implications of New OSL Dates on the Formation of the "Shell Bar" in the Qaidam Basin, Northeastern Qinghai-Tibetan Plateau. *J. Palaeolimnology* 51, 197–210. doi: 10.1007/s10933-013-9710-1

Li, S. Q., Li, S. L., Chen, Z. X., Tang, B. G., and Chen, Y. X. (2002a). Deltaic Sedimentary Sequences Developed During Last Glacial Maximum in the EA01 Core on the Outer Shelf of the East China Sea. *Mar. Geol. Quat. Geol.* 22 (3), 19–26. doi: 10.16562/j.cnki.0256-1492.2002.03.003

Li, C. X., Wang, P., Sun, H. P., Zhang, J. Q., Fan, D. D., and Deng, B. (2002b). Late Quaternary Incised-Valley Fill of the Yangtze Delta (China), its Stratigraphic Framework and Evolution. *Sediment. Geol.* 152, 133–158. doi: 10.1016/S0037-0738(02)00066-0

Li, G. X., Li, P., Liu, Y., Qiao, L. L., Ma, Y. Y., Xu, J. S., et al. (2014a). Sedimentary System Response to the Global Sea Level Change in the East China Seas Since the Last Glacial Maximum. *Earth Sci. Rev.* 139, 390–405. doi: 10.1016/j.earscirev.2014.09.007

Li, Z. Y., Liu, D. S., and Long, H. Y. (2014b). Living and Dead Benthic Foraminifera Assemblages in the Bohai and Northern Yellow Seas: Seasonal Distributions and Paleoenvironmental Implications. *Quat. Int.* 349, 113–126. doi: 10.1016/j.quaint.2014.05.019

Li, G. X., Liu, Y., and Yang, Z. G. (2009). Sea Level Rise and Sea Sedimentary Environment Response in the East China Continental Shelf Since the Last Glacial Maximum. *Mar. Geol. Quat. Geol.* 29 (4), 13–19. doi: 10.3724/SP.J.1140.2009.04013

Li, G. X., Liu, Y., Yang, Z. G., Yue, S. H., Yang, W. D., and Han, X. B. (2005a). Ancient Changjiang Channel System in the East China Sea Continental Shelf During the Last Glaciation. *Sci. China (Ser. D: Earth Sci.)* 48 (11), 1972–1978. doi: 10.1360/04yd0053

Lin, H. L., and Hsieh, H. Y. (2007). Seasonal Variations of Modern Planktonic Foraminifera in the South China Sea. *Deep-Sea Res. Part II* 54, 1634–1644. doi: 10.1016/j.dsr2.2007.05.007

Liu, Z. X., Berné, S., Saito, Y., Lerricolais, G., and Marsset, T. (2000). Quaternary Seismic Stratigraphy and Paleoenvironments on the Continental Shelf of the East China Sea. *J. Asian Earth Sci.* 18, 441–452. doi: 10.1016/S1367-9120(99)00077-2

Liu, Z. X., Berné, S., Saito, Y., Yu, H., Trentesaux, A., Uehara, K., et al. (2007a). Internal Architecture and Mobility of Tidal Sand Ridges in the East China Sea. *Cont. Shelf Res.* 27, 1820–1834. doi: 10.1016/j.csr.2007.03.002

Liu, Z. X., Berné, S.the L'ATALANTE Party (1999). Paleo-Environment in the Continental Shelf of the East China Sea Since the Mid-Pleistocene (in Chinese With English Abstract). *Mar. Geol. Quat. Geol.* 19 (2), 1–10. doi: 10.16562/j.cnki.0256-1492.1999.02.001

Liu, J. P., and Milliman, J. D. (2004a). Reconsidering Melt-Water Pulses 1A and 1B: Global Impacts of Rapid Sea-Level Rise. *J. Ocean Univ. China* 3 (3), 183–190. doi: 10.1007/s11802-004-0033-8

Liu, J. P., Milliman, J. D., Gao, S., and Cheng, P. (2004b). Holocene Development of the Yellow River's Subaqueous Delta, North Yellow Sea. *Mar. Geol.* 209 (1–4), 45–67. doi: 10.1016/j.margeo.2004.06.009

Liu, J., Saito, Y., Kong, X. H., Wang, H., Xiang, L. H., Wen, C., et al. (2010). Sedimentary Record of Environmental Evolution Off the Yangtze River Estuary, East China Sea, During the Last 13, 000 Years, With Special Reference to the Influence of the Yellow River on the Yangtze River Delta During Last 600 Years. *Quat. Sci. Rev.* 29, 2424–2438. doi: 10.1016/j.quascirev.2010.06.016

Liu, J. X., Shi, X. F., Liu, Q., Liu, S., Liu, Y., Zhang, Q., et al. (2021). Authigenic Iron Sulfides Indicate Sea-Level Change on the Continental Shelf: An Illustration From the East China Sea. *J. Geophys. Res. Solid Earth* 126, e2020JB021222 . doi: 10.1029/2020JB021222

Liu, J. G., Xiang, R., Chen, M. H., Chen, Z., Yan, W., and Liu, F. (2011). Influence of the Kuroshio Current Intrusion on Depositional Environment in the Northern South China Sea: Evidence From Surface Sediment Records. *Mar. Geol.* 285, 59–68. doi: 10.1016/j.margeo.2011.05.010

Liu, J. P., Xu, K. H., Li, A. C., Milliman, J. D., Velozzi, D. M., Xiao, S. B., et al. (2007b). Flux and Fate of Yangtze River Sediment Delivered to the East China Sea. *Geomorphology* 85, 208–224. doi: 10.1016/j.geomorph.2006.03.023

Liu, Z. X., Yin, P., Xiong, Y. Q., Berné, S., Trentesaux, A., and Li, C. X. (2003). Quaternary Transgressive and Regressive Depositional Sequences in the East China Sea. *Chin. Sci. Bull.* 48 (S), 81–87. doi: 10.1007/BF02900944

Li, G. X., Yang, Z. G., and Liu, Y. (2005b). *The Environmental Formation Map of the Seabed Sediments in the East China Marginal Sea* (Beijing: Science Press), 17–29.

Lobo, F. J., and Ridente, D. (2014). Stratigraphic Architecture and Spatio-Temporal Variability of High-Frequency (Milankovitch) Depositional Cycles on Modern Continental Margins: An Overview. *Mar. Geol.* 352, 215–247. doi: 10.1016/j.margeo.2013.10.009

Marsset, T., Xia, D. X., Berné, S., Liu, Z. X., Bourillet, J. F., and Wang, K. Y. (1996). Stratigraphy and Sedimentary Environments During the Late Quaternary in the Eastern Bohai (North China Platform). *Mar. Geol.* 135 (1–4), 97–114. doi: 10.1016/S0025-3227(96)00038-2

Martinson, D. G., Pisias, N. G., Hays, J. D., Imbrie, J., Moore, T. C., and Shackleton, N. J. (1987). Age Dating and the Orbital Theory of the Ice Ages: Development of a High-Resolution 0 to 300,000 Year Chronostratigraphy. *Quat. Res.* 27, 1–29. doi: 10.1016/0033-5894(87)90046-9

Mei, X., Li, R. H., Zhang, X. H., Liu, Q. S., Liu, J. X., Wang, Z. B., et al. (2016). Evolution of the Yellow Sea Warm Current and the Yellow Sea Cold Water Mass Since the Middle Pleistocene. *Palaeogeogr. Palaeoclimatol. Palaeoecol.* 442, 48–60. doi: 10.1016/j.palaeo.2015.11.018

Murray, A. S., and Wintle, A. G. (2003). The Single Aliquot Regenerative Dose Protocol: Potential for Improvements in Reliability. *Radiat. Meas.* 37, 377–381. doi: 10.1016/S1350-4487(03)00053-2

Neal, J., and Abreu, V. (2009). Sequence Stratigraphy Hierarchy and the Accumulation Succession Method. *Geology* 37 (9), 779–782. doi: 10.1130/G25722A.1

Pigati, J. S., Quade, J., Wilson, J., Jull, A. T., and Lifton, N. A. (2007). Development of Low-Background Vacuum Extraction and Graphitization Systems for ^{14}C Dating of Old (40–60 Ka) Samples. *Quat. Int.* 166, 4–14. doi: 10.1016/j.quaint.2006.12.006

Prescott, J. R., and Hutton, J. T. (1994). Cosmic Ray Contributions to Dose Rates for Luminescence and ESR Dating: Large Depths and Long-Term Time Variations. *Radiat. Meas.* 23, 497–500. doi: 10.1016/1350-4487(94)90086-8

Qin, Y. S., Chen, L. R., Zhao, Y. Y., and Zhao, S. L. (1987). Geology of the East China Sea. (Beijing: Science Press), 130–151.

Reimer, P. J., Austin, W. E., Bard, E., Bayliss, A., Blackwell, P. G., Ramsey, C. B., et al. (2020). The IntCal20 Northern Hemisphere Radiocarbon Age Calibration Curve (0–55 Cal kBP). *Radiocarbon.* 62, 725–757. doi: 10.1017/RDC.2020.41

Saito, Y. (1998a). Sea Levels of the Last Glacial in the East China Sea Continental Shelf. *Quaternary Res. (Daiyonki Kenkyu)* 37, 237–242. doi: 10.4116/jaqua.37.235

Saito, Y., Katayama, H., Ikehara, K., Kato, Y., Matsumoto, E., Oguri, K., et al. (1998b). Transgressive and Highstand Systems Tracts and Post-Glacial

Transgression, the East China Sea. *Sediment. Geol.* 122, 217–232. doi: 10.1016/S0037-0738(98)00107-9

Shannon, C. E., and Wiener, W. (1949). *The Mathematical Theory of Communication* (Urbana: The University of Illinois Press), 117.

Siddall, M., Rohling, E. J., Almogi-Labin, A., Hemleben, C., Meischner, D., Schmelzer, I., et al. (2003). Sea-Level Fluctuations During the Last Glacial Cycle. *Nature* 423 (6942), 853–858. doi: 10.1038/nature01690

Siddall, M., Rohling, E. J., Thompson, W. G., and Waelbroeck, C. (2008). Marine Isotope Stage 3 Sea Level Fluctuations: Data Synthesis and New Outlook. *Rev. Geophys.* 46 (4), 171–200. doi: 10.1029/2007RG000226

Song, Y. G., Lai, Z. P., Li, Y., Chen, T., and Wang, Y. X. (2015). Comparison Between Luminescence and Radiocarbon Dating of Late Quaternary Loess From the Ili Basin in Central Asia. *Quaternary Geochronology* 30, 405–410. doi: 10.1016/j.quageo.2015.01.012

Su, D. P., Hu, G., Liu, J., and Zhang, X. J. (2008). Hydrodynamic Study of the Tidal Sand Ridges on the Shelf of the East China Sea (in Chinese With English Abstract). *Mar. Geol. Lett.* 24 (6), 15–18. doi: 10.16028/j.1009-2722.2008.06.004

Tang, B. G. (1996). "Quaternary Stratigraphy on the Shelf of the East China Sea," in *Quaternary Stratigraphy in China and its International Correlation*. Eds. Z. G. Yang and H. M. Liu (Beijing: Geological Publishing House), 56–75.

Uehara, K., and Saito, Y. (2003). Late Quaternary Evolution of the Yellow/East China Sea Tidal Regime and its Impact on Sediment Dispersal and Seafloor Morphology. *Sediment. Geol.* 162, 25–38. doi: 10.1016/S0037-0738(03)00234-3

Uehara, K., Saito, Y., and Hori, K. (2002). Paleotidal Regime in the Changjiang (Yangtze) Estuary, the East China Sea at 6 and 10 Ka Estimated From a Numerical Model. *Mar. Geol.* 183 (1-4), 179–192. doi: 10.1016/S0025-3227(01)00255-9

Ujiie, Y., Ujiie, H., Taira, A., Nakamura, T., and Oguri, K. (2003). Spatial and Temporal Variability of Surface Water in the Kuroshio Source Region, Pacific Ocean, Over the Past 21,000 Years: Evidence From Planktonic Foraminifera. *Mar. Micropaleontol.* 49, 335–364. doi: 10.1016/S0377-8398(03)00062-8

Waelbroeck, C., Labeyrie, L., Michel, E., Duplessy, J. C., McManus, J. F., Lambeck, K., et al. (2002). Sea-Level and Deep Water Temperature Changes Derived From Benthonic Foraminifera Isotopic Records. *Quaternary Sci. Rev.* 21, 295–305. doi: 10.1016/S0277-3791(01)00101-9

Wang, P. X., Min, Q. B., and Bian, Y. H. (1987). Distribution of Planktonic Foraminifera in Surface Sediments of the East China Sea and the Huanghai Sea. *Acta Sedimentol. Sin.* Supp (6), 225–230.

Wang, Z. H., Saito, Y., Hori, K., Kitamura, A., and Chen, Z. Y. (2005). Yangtze Offshore, China: Highly Laminated Sediments From the Transition Zone Between Subaqueous Delta and the Continental Shelf. *Estuarine Coastal Shelf Sci.* 62, 161–168. doi: 10.1016/j.ecss.2004.08.012

Wang, Z. B., Yang, S. Y., Wang, Q., Zhang, Z. X., Zhang, X. H., Lan, X. H., et al. (2014). Late Quaternary Stratigraphic Evolution on the Outer Shelf of the East China Sea. *Cont. Shelf Res.* 90, 5–16. doi: 10.1016/j.csr.2014.04.015

Wang, Z. B., Yang, S. Y., Zhang, Z. X., Lan, X. H., Gu, Z. F., and Zhang, X. H. (2013). Paleo-Fluvial Sedimentation on the Outer Shelf of the East China Sea During the Last Glacial Maximum. *Chin. J. Oceanol. Limnol.* 31 (4), 886–894. doi: 10.1007/s00343-013-2253-5

Wang, P. X., Zhang, J. J., and Min, Q. B. (1985). "Distribution of Foraminifera in Surface Sediments of the East China Sea," in *Marine Micropaleontology of China*. Ed. P. X. Wang (Beijing: China Ocean Press & Springer-Verlag), 34–69.

Wang, P. X., Zhang, J. J., and Zhao, Q. H. (1988). *Foraminifera and Ostracodes in Surface Sediments of the East China Sea* (Beijing: China Ocean Press), 34–60.

Wellner, R. W., and Bartek, L. R. (2003). The Effect of Sea Level, Climate, and Shelf Physiography on the Development of Incised-Valley Complexes: A Modern Example From the East China Sea. *J. Sediment. Res.* 73, 926–940. doi: 10.1306/041603730926

Winkler, M. G., and Wang, P. K. (1993). "Late-Quaternary Vegetation and Climate in China," in *Global Climates Since the Last Glacial Maximum*. Eds. H. E. Wright, J. E. Kutzbach, T. Webb, W. F. Ruddiman, F. A. Street-Perrott and P. J. Bartlein (London: University of Minnesota Press), 221–253.

Woodroffe, C. D., Mulrennan, M. E., and Chappell, J. (1993). Estuarine Infill and Coastal Progradation, Southern Van Diemen Gulf, Northern Australia. *Sediment. Geol.* 83, 257–275. doi: 10.1016/0037-0738(93)90016-X

Wu, Z. Y., Jin, X. L., Cao, Z. Y., Li, J. B., Zheng, Y. L., and Shang, J. H. (2010). Distribution, Formation and Evolution of Sand Ridges on the East China Sea Shelf. *Sci. China (Ser. D: Earth Sci.)* 53, 101–112. doi: 10.1007/s11430-009-0190-0

Wu, Z. Y., Jin, X. L., Li, J. B., Zhen, Y. L., and Wang, X. B. (2005). Linear Sand Ridges on the Outer Shelf of the East China Sea. *Chin. Sci. Bull.* 50 (21), 2517–2528. doi: 10.1007/BF03183643

Xu, Y. T., Lai, Z. P., and Li, C. A. (2019). Sea Level Determined Lake Formation in the Yangtze Plain- A Review. *Global Planetary Change* 181, 102980. doi: 10.1016/j.gloplacha.2019.102980

Xu, X. L., Li, H. W., Tang, L. J., Lai, Z. P., Xu, G. J., Zhang, X. H., et al. (2020). Chronology of a Holocene Core From the Pearl River Delta in Southern China. *Front. Earth Sci.* 8, 262. doi: 10.3389/feart.2020.00262

Xu, T. Y., Shi, X. F., Liu, S. F., Qiao, S. Q., Yao, Z. Q., Fang, X. S., et al. (2018). Late Quaternary Sedimentary Evolution of the Outer Shelf of the East China Sea. *Quat. Int.* 493, 59–69. doi: 10.1016/j.quaint.2018.06.043

Xu, T. Y., Shi, X. F., Liu, C. G., Wu, Y. H., Liu, S. F., Fang, X. S., et al. (2020). Stratigraphic Framework and Evolution of the Mid-Late Quaternary (Since Marine Isotope Stage 8) Deposits on the Outer Shelf of the East China Sea. *Mar. Geol.* 419, 106047. doi: 10.1016/j.margeo.2019.106047

Yang, C. S. (1989). Active, Moribund and Buried Tidal Sand Ridges in the East China Sea and the Southern Yellow Sea. *Mar. Geol.* 88, 97–116. doi: 10.1016/0025-3227(89)90007-8

Yang, W. D. (2002). Structure and Sedimentary Environment for Submarine Dune Ridges in the East China Sea (in Chinese With English Abstract). *Mar. Geol. Quat. Geol.* 22, 9–16.

Yang, S. Y., Bi, L., Li, C., Wang, Z. B., and Dou, Y. G. (2016). Major Sinks of the Changjiang (Yangtze River)-Derived Sediments in the East China Sea During the Late Quaternary. *Geological Soc. Lond. special Publ. River-Dominated Shelf Sediments East Asian Seas* 429, 137–52. doi: 10.1144/SP429.6

Yang, Z. G., Lin, H. M., Wang, S. J., and Li, S. Q. (1998). A Study of the Ancient Cold Water Mass Sediments in South Yellow Sea During Last Interglacial (in Chinese With English Abstract). *Mar. Geol. Quat. Geol.* 18 (1), 47–58.

Yang, Z. G., Lin, H. M., and Zhang, G. W. (1996). "Quaternary Stratigraphy in the Shelf of the Yellow Sea," in *Quaternary Stratigraphy in China and its International Correlation*. Eds. Z. G. Yang and H. M. Lin (Beijing: Geological Publishing House), 31–55.

Yang, S. Y., Wang, Z. B., Dou, Y. G., and Shi, X. F. (2014). "A Review of Sedimentation Since the Last Glacial Maximum on the Continental Shelf of Eastern China," in *Continental Shelves of the World: Their Evolution During the Last Glacio-Eustatic Cycle*, vol. 41 . Eds. F. L. Chiocci and A. R. Chivas (London: Geological Society of London, Memoir), 293–303.

Yoneda, M., Uno, H., Shibata, Y., Suzuki, R., Kumamoto, Y., Yoshida, K., et al. (2007). Radiocarbon Marine Reservoir Ages in the Western Pacific Estimated by Pre-Bomb Molluscan Shells. *Nucl. Instrum. Methods Phys. Res. B* 259, 432–437. doi: 10.1016/j.nimb.2007.01.184

Yoo, D. G., Lee, C. W., Kim, S. P., Jin, J. H., and Han, H. C. (2002). Late Quaternary Transgressive and Highstand Systems Tracts in the Northern East China Sea Mid-Shelf. *Mar. Geol.* 187, 313–328. doi: 10.1016/S0025-3227(02)00384-5

Yu, H., Liu, Z. X., Xiong, Y. G., Li, S. L., and Xiang, R. (2006). Stratigraphy of Core EA05 From Southern East China Sea Continental Shelf Since the Last Glacial Maximum and its Paleo-Environment Implication. *Peri. Ocean Univ. China* 36 (4), 545–550. doi: 10.1007/s11769-006-0026-1

Zhao, B. C., Wang, Z. H., Chen, J., and Chen, Z. Y. (2008). Marine Sediment Records and Relative Sea Level Change During Late Pleistocene in the Changjiang Delta Area and Adjacent Continental Shelf. *Quat. Int.* 186, 164–172. doi: 10.1016/j.quaint.2007.08.006

Zhen, Z. G., Zhong, W., Xue, J. B., Zheng, Y. M., and Liu, W. (2008). Progress in the Studies of Climatic Features in Different Areas of China During the MIS-3 (in Chinese With English Abstract) . *J. Glaciol. Geocryol.* 30 (5), 814–824.

Zhu, Y. Q., Li, C. Y., Zeng, C. K., and Li, B. G. (1979). Lowest Sea Level About the Continental Shelf of the East China Sea During Late Pleistocene (in Chinese With English Abstract). *Chin. Sci. Bull.* 7, 317–320.

Conflict of Interest: The authors declare that the research was conducted in the absence of any commercial or financial relationships that could be construed as a potential conflict of interest.

this article, or claim that may be made by its manufacturer, is not guaranteed or endorsed by the publisher.